Politecnico di Torino

Porto Institutional Repository

[Article] Modelling the swelling and osmotic properties of clay soils. Part II: The physical approach

(Article begins on next page)
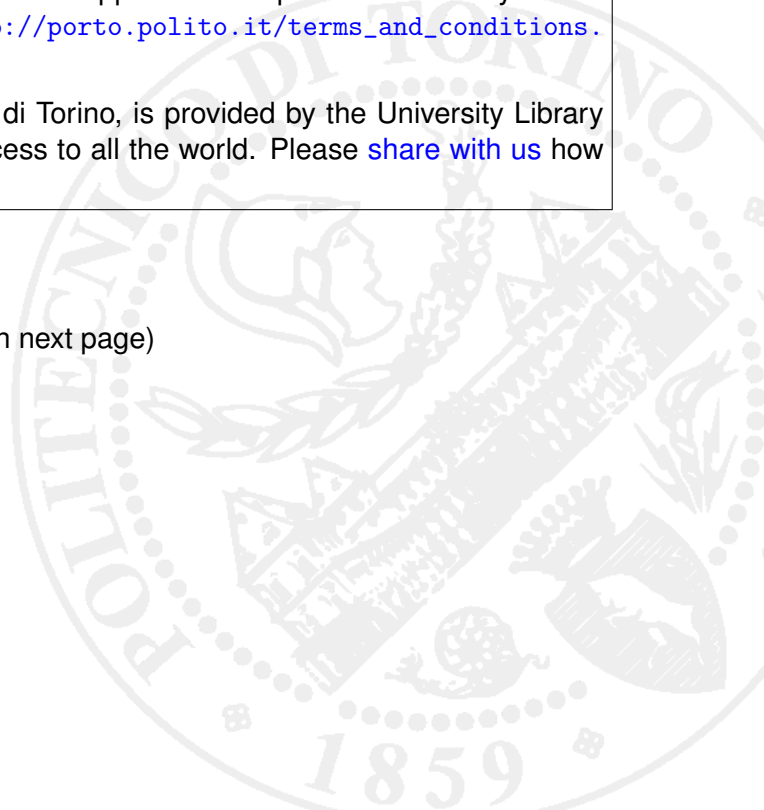
Modelling the swelling and osmotic properties of clay soils: Part II. The physical approach

by

Andrea Dominijanni* and Mario Manassero**

*   *Corresponding Author*

     Dipartimento d'Ingegneria del Territorio, dell'Ambiente e delle Geotecnologie [Land, Environment and Geo-Engineering Department], Politecnico di Torino, Corso Duca degli Abruzzi 24, 10129 Torino – ITALY; Ph: +39-011-090-7705, Fax: +39-011-090-7699, Cell Ph: +39-3387778804; e-mail: andrea.dominijanni@polito.it

**   Dipartimento d'Ingegneria del Territorio, dell'Ambiente e delle Geotecnologie [Land, Environment and Geo-Engineering Department], Politecnico di Torino, Corso Duca degli Abruzzi 24, 10129 Torino – ITALY; Ph: +39-011-090-7705, Fax: +39-011-090-7699, e-mail: mario.manassero@polito.it

ABSTRACT

The increasing use of clays, with a high montmorillonite content in their mineralogical composition, as hydraulic and contaminant barriers for landfill and soil remediation applications needs to be supported by an adequate theoretical modelling of the mechanical behaviour and transport properties, in order to assess the expected performances in the long term. The framework of the thermodynamics of irreversible processes was adopted in a companiom paper to derive phenomenological constitutive equations for a clay soil characterized by swelling and osmotic phenomena, without specifying any of the physical mechanisms that occur at the pore scale. In this paper, a *physical* approach is proposed in order to provide an interpretation of the phenomenological parameters, obtained from laboratory tests. The soil structure is assumed to be constituted by montmorillonite lamellae,

that can be aggregated to form the so-called tactoids, which have a slit-like geometry. Chemical equilibrium is assumed to be established between the bulk electrolyte solutions and the internal pore solution at the macroscopic scale, so that the hydraulic pressure and ion concentrations can be evaluated through the Donnan equations. Water and ion transport is described at the pore scale through the generalized Navier-Stokes equation and the generalized Nernst-Planck equations, respectively. Mechanical behaviour is modelled taking into account intergranular contact stresses. The approach is applied to interpret literature experimental results, showing how it can reduce the number of tests that need to be carried out and provide insight into the physical mechanisms that determine the observed phenomena.

INTRODUCTION

Clay soils with a high montmorillonite content are increasingly used as hydraulic and contaminant barriers, due to the their low hydraulic conductivity, k, to permeation with water and dilute aqueous solutions (k typically $\leq 3.0 \cdot 10^{-11}$ m/s). Bentonite, which is a clay mixture that contains about 70% of montmorillonite, is currently used in the so-called geosynthetic clay liners (GCLs), which have been proposed as an alternative to traditional clay compacted liners, due to their reduced costs and ease of installation. GCLs are factory manufactured products that consist of a thin layer of bentonite (5÷10 mm thick) sandwiched between two geotextiles.

Bentonite is characterized by the swelling and osmotic phenomena that are typical of polyelectrolyte gels and biological membranes, and which is attributed to the interaction between the electric charge of montmorillonite lamellae and the ions contained in the pore solution.

In order to account for these phenomena specific theoretical approaches need to be developed to assess the long-term behaviour of barriers containing bentonite.

A first fundamental distinction can be made between *phenomenological* approaches, which only have the aim of describing *how* phenomena occur, and *physical* approaches, which, on the basis of a conceptual picture of the physical and chemical interactions between the solid and liquid phases at the soil pore scale, have the scope of explaining *why* phenomena occur.

In Dominijanni and Manassero (2011), the phenomenological approach was developed using the formalism of the thermodynamics of irreversible processes (Eckart, 1940a,b; Coussy, 1995 and 2004), in order to derive transport and poro-elastic constitutive equations. The analysis referred to a pore solution containing N ion species, with the following simplifying assumptions:

1. unidimensional geometry;

2. infinitesimal strains of the solid skeleton;

3. saturated porous medium;

4. incompressible solid and liquid phase;

5. infinitely diluted electrolyte solution;

6. complete dissociation of the salts in the solution;

7. absence of chemical reactions.

In order to maintain the purely phenomenological approach, i.e. without any specification of the physical and chemical phenomena that occur at the pore scale, it was necessary to refer the state variables of the system (i.e. the hydraulic pressure, the ion concentrations and the electric potential) to a virtual solution, which was considered to be in thermodynamic equilibrium with the real pore solution at any point of the porous medium. The consistency of such an approach was assured by the possibility of formulating the boundary conditions for the virtual solution, in terms of the values assumed by the state variables in the external real bulk solutions in contact with the porous medium.

The obtained constitutive equations were characterized by a defined number of parameters (called phenomenological parameters), subject to some restrictions due to the Clausius-Duhem inequality. These parameters were assumed to be measured by means of macroscopic experimental tests, without any identification of the physical mechanisms at the microscopic scale that influence them.

However, a practical shortcoming of the approach was the very high number of tests necessary to characterized a single bentonite, due to the dependency of the phenomenological parameters on the state variables.

The limitations implied by the lack of a physical interpretation of the mechanisms that generate the phenomena observed at the macroscopic scale were also empathized.

In this paper, a theoretical model is developed following the physical approach in order to provide an interpretation of the phenomenological parameters introduced in Dominijanni and Manassero (2011).

From a historical point of view, the physical approach is older than the phenomenological one, and it dates back to the pioneering works of von Helmholtz and Smoluchowski on electrokinetic phenomena in fine capillaries (Lyklema, 2003). The aim of these eminent scientists was to explain macroscopic phenomena, such as electro-osmosis, that is, the flow of water driven by an electric potential gradient, on the basis of the electrostatic interaction between the charged wall of a capillary pore and the ions in the solution within the capillary. Their theory was later revised by Gouy (1910) and Chapman (1913), who were the first to evaluate the distribution of the electric potential in a charged pore by solving the Poisson-Boltzmann equation. The Gouy-Chapman theory represents the mathematical formulation of the simplest double diffuse layer (DDL) model, which has been named in such a way because it is based on an idealized picture of the distribution of electric charges in the pore, where the first layer of electric charges is given by the solid wall of the pore and the second layer is represented by the ions contained in the pore solution. A relevant improvement in such a model was given by Stern (1924), who accounted for the presence of a layer of specifically adsorbed ions on the pore wall surface.

Gross and Osterle (1968) coupled the Gouy-Chapman theory to transport equations in order to model the motion of electrolyte solutions through charged porous media and Groenevelt and Bolt (1969) applied this model to bentonites. In this theoretical approach, the microscopic equations are upscaled to the macroscopic scale of observation through the method of volume averaging. In such a way, a macroscopic interpretation is provided of the transport parameters, starting from the evaluation of the interaction between the solid skeleton and the pore solution at the pore scale.

Recently, Moyne an Murad (2002) extended the approach to the evaluation of the mechanical behaviour of the solid skeleton by adopting a homogenization procedure in order to upscale the constitutive equations from the pore to the macroscopic scale.

The main difficulty involved in applying DDL is that it needs the non-linear Poisson-Boltzmann equation to be solved in the microscopic porous medium unit cell. Owing to the high non-linearity of this equation, only numerical solutions can be found and these do not provide explicit relations with the state variables.

A simpler theory, based on the approximation of considering only the equilibrium between phases at the macroscopic scale, was developed by Donnan (1911) and was the applied to transport processes across membranes by Teorell (1935, 1937), Meyer and Sievers (1936a,b), Kedem and Katchalsky (1961) and Hoffer and Kedem (1967). This theory can also be used to determinate the swelling pressure (Dähnert and Huster, 1999). In this model, the Poisson-Boltzmann equation is averaged across the pore and reduced to the electroneutrality condition in the presence of a solid skeleton charge. This theory was applied to the evaluation of clay soil transport properties by Hanshaw and Coplen (1973), Marine and Fritz (1981), Muurinen et al. (2004), Revil and Leroy (2004), Revil at al. (2005), Leroy et al. (2006) and Birgersson and Karnland (2009).

In this paper, the approach is extended to also include the mechanical behaviour of the solid skeleton and is applied to interpret the phenomenological parameters derived in the companion paper (Dominijanni and Manassero, 2011).

BENTONITE STRUCTURE

Bentonite is a clay soil that usually contains about 70% of the three layered (2:1) clay mineral called montmorillonite. Isomorphic substitution in montmorillonite usually results in the replacement of a portion of trivalent aluminum (Al^{3+}) in the crystalline structure with a divalent metal, such as magnesium (Mg^{2+}), and this leads to a negative surface charge. The ideal unit cell formula of montmorillonite is {$(OH)4Si8Al3.44Mg0.66O20 \cdot nH2O0.66-$} with a typical surface charge of 0.66 equivalent per unit cell. Montmorillonite crystals consist of parallel-aligned elementary alumino-silicate lamellae, which are approximately 10 Å thick and 1000-2000 Å in the lateral extent. The unit cell parameters are a = 5.17 Å and b = 8.95 Å, which correspond to a unit cell area of 92.5 $Å^2$, or one unit charge per 140 $Å^2$. The corresponding surface charge, σ, is equal to 0.114 $C \cdot m^{-2}$. The total specific surface, S, available for water adsorption is approximately equal to 760 $m^2 \cdot g^{-1}$, assuming a solid density, $\rho_{sk} = 2.65$ $g \cdot cm^{-3}$.

Montmorillonite particles can be represented as infinitely extended platy particles. The half distance, b (m), between the montmorillonite particles can be estimated from the total porosity, n (-), or the void ratio, e = n/(1−n) (-). Norrish (1954) showed that bentonite can have a dispersed structure in which clay particles are present, as well separated units, or an aggregated structure that consists of packets of particles, or tactoids, within which several clay platelets or lamellae are in a parallel array, with a characteristic interparticle distance of 9 Å.

The formation of tactoid has the net result of reducing the surface area of the montmorillonite, which then behaves like a much larger particle with the diffuse double layer only fully manifesting itself on the outside surfaces of the tactoids (see Fig. 1). The formation of tactoids is due to internal flocculation of the clay platelets, and depends on the concentration and the valence of the ions in the soil solution. The number, N_l, of clay platelets or lamellae forming

tactoids increases with an increase of the ion concentration and valence of cations in the soil solution. Unfortunately, the number of platelets in a tactoid cannot be predicted and has to be estimated from macroscopic measurements of the transport parameters (e.g. hydraulic conductivity). A complicating factor is the non-uniform distribution of ions in mixed systems. For instance, in Na^+-Ca^{2+} systems, the distribution of the ions is not random, but the charges within the tactoids are mainly neutralized by Ca^{2+}, whereas those on the outer surfaces are substantially enriched in Na^+ over Ca^{2+}.

The average half spacing, b, in dispersed clays may be estimated assuming a uniform distribution of the clay platelets in a parallel orientation, from the relation:

$$b = \frac{e}{\rho_{sk} S} \tag{1}$$

If the clay has an aggregated structure, only the external surface of the tactoids is in contact with the mobile fluid, therefore the void space within the platelets in the tactoids should be subtracted from the total void space to obtain the void space with reference to the conducting pores (see Fig. 1). If N_1 is the number of platelets per tactoid, the external specific surface, S', and the internal specific surface, S'', are given by:

$$S' = \frac{S}{N_1} \tag{2a}$$

$$S'' = S - S' = \frac{(N_1 - 1)}{N_1} S. \tag{2b}$$

The average half spacing between the platelets in the tactoids, as determined by means of X-ray measurements, is $b'' = 4.5$ Å (Shainberg et al., 1971). The total void index, e_T, of the

bentonite is given by the sum of the void index inside the tactoid, e'', and the void index, e, of the conducting pores. The water in the tactoids can be considered part of the solid particles and is excluded from the transport mechanisms.

The void index associated with the internal surfaces of the tactoid, e'', can be estimated as follows:

$$e'' = b'' \rho_{sk} S''. \tag{3}$$

where ρ_{sk} = density of the solid particles (kg/m^3).

The corrected half spacing, b, between the tactoids, in the case of an aggregate microstructure of bentonite, can be estimated from a similar equation to Eq.1:

$$b = \frac{e}{\rho_{sk} S'} \tag{4}$$

where $e = e_T - e_0$ = void ratio reffering to the void space between the tactoids and S' = effective specific surface of the tactoids.

When the number, N_l, of clay platelets in the tactoids increases, the external specific surface decreases and the half spacing, b, between the tactoids increases, even though the total void ratio remains constant and the void ratio referring to the pore volume available for the transport decreases.

Guyonnet et al. (2005), through a comparison of the results of hydraulic conductivity tests and microscopic analyses of bentonite structure based on small angle X-ray scattering and transmission electron microscopy, showed that high values of the hydraulic conductivity are related to an aggregated structure (also called the hydrated-solid phase), while low values of

the hydraulic conductivity are related to a dispersed structure (also called the gel phase). These experimental results can be explained by the increase in the average pore size, due to tactoid formation (see Fig. 1).

PARTITION EFFECT

On the basis of the previous description of the micro-structure of bentonite, the pores in the clay may be considered as capillaries with a slit-like geometry. When such a porous medium is interposed between two solutions of different electrolyte concentrations, the internal surface of the pore acquires a charge, and electric double layers develop within the pore. A rectangular coordinate system (x,y) is used to describe the flow, where x is the position along the longitudinal axis of the pore, while y is the distance from the central axis in the transversal direction (see Fig. 2).

At the microscopic scale, the variables of the physical system are indicated as $\bar{u}^{micro}, \bar{c}_i^{micro}, \bar{\varphi}^{micro}$, and these represent the hydraulic pressure, the ion concentrations and the electric potential, respectively. These microscopic variables are related to the corresponding macroscopic quantities through volume averaging over the capillary cross-section, i.e.

$$\bar{u} = \left\langle \bar{u}^{micro} \right\rangle \tag{5a}$$

$$\bar{c}_i = \left\langle \bar{c}_i^{micro} \right\rangle \tag{5b}$$

$$\bar{\varphi} = \left\langle \bar{\varphi}^{micro} \right\rangle \tag{5c}$$

where the brackets mean averaging over the capillary cross section, i.e. $\left\langle \bullet \right\rangle = \frac{1}{b} \int_0^b \bullet \, dy$.

The variable symbols are over-marked to show that they refer to the real pore solution and not to the corresponding virtual solution adopted in the phenomenological approach (Dominijanni and Manassero, 2011). The hydraulic pressure, the ion concentrations and the electric potential of the virtual solution, which is in thermodynamic equilibrium with the real pore solution at the generic position x in the porous medium, are indicated as u, c_i and φ,

respectively. The virtual variables do not depend on the microscopic variable y and, as a result, do not vary when they are upscaled from the microscopic to the macroscopic scale.

The real electric potential at the microscopic scale $\overline{\varphi}^{micro}(x,y)$ can be assumed, according to Gross and Osterle (1968) and Yaroshchuk (1995), as being composed of two parts: the first, $\overline{\psi}^{micro}(x,y)$ represents the electric potential due to the double layer, while the second, $\varphi(x)$, denotes the potential of a virtual bulk solution that is in thermodynamic equilibrium with the soil solution at the generic position x.

The total electric potential in the pore satisfies the Poisson equation:

$$\nabla^2\overline{\varphi}^{micro} = -\frac{F}{\varepsilon_r\varepsilon_0}\sum_{i=1}^{N}z_i\overline{c}_i^{micro} \tag{6}$$

where

F = Faraday's constant (96,485 C·mol^{-1});

ε_r = relative permittivity (for water, ε_r = 78);

ε_0 = vacuum permittivity (8.854·10^{-12} C·V^{-1}·m^{-1});

z_i = elctro-chemical valence of the i-th ion.

Since the length of the pores is much longer than the transversal spacing (L >> b), the axial variations of the potential may be neglected with respect to the transversal ones:

$$\frac{d^2\overline{\psi}^{micro}}{dy^2} = -\frac{F}{\varepsilon_r\varepsilon_0}\sum_{i=1}^{N}z_i\overline{c}_i^{micro} \ . \tag{7}$$

The Poisson equation is usually associated to the following boundary conditions:

$$\frac{d\overline{\psi}^{micro}}{dy}(y=0)=0 \text{ at the centre of the pore} \qquad (8a)$$

$$\frac{d\overline{\psi}^{micro}}{dy}(y=b)=-\frac{\sigma_d}{\varepsilon_r\varepsilon_0} \text{ at the clay surface} \qquad (8b)$$

where σ_d = electric surface charge associated to the diffuse double layer ($C\cdot m^{-2}$). σ_d is given by the total surface charge, σ, minus the surface charge in the Stern layer σ_{Stern}, i.e. $\sigma_d = \sigma - \sigma_{Stern}$.

Using the boundary conditions Eqs. 8, the area average of Eq. 7 may be expressed as follows (Cwirko and Carbonell, 1988; Moyne and Murad, 2002):

$$\int_0^b \frac{d^2\overline{\psi}^{micro}}{dy^2} = -\int_0^b \frac{F}{\varepsilon_0\varepsilon_r}\sum_{i=1}^N z_i\overline{c}_i^{micro}$$

$$\frac{d\overline{\psi}^{micro}}{dy}\bigg|_{y=b} - \frac{d\overline{\psi}^{micro}}{dy}\bigg|_{y=0} = -\frac{F}{\varepsilon_0\varepsilon_r}\sum_{i=1}^n z_i\int_0^b \overline{c}_i^{micro}$$

$$-\frac{\sigma_d}{\varepsilon_0\varepsilon_r} - 0 = -\frac{F}{\varepsilon_0\varepsilon_r}b\sum_{i=1}^N z_i\overline{c}_i$$

$$\sum_{i=1}^N z_i\overline{c}_i = \frac{\sigma_d}{F\cdot b} = \overline{c}_{sk} \qquad (9)$$

where

$\overline{c}_{sk}$ = solid skeleton charge concentration referring to the pore volume ($mol\cdot m^{-3}$).

Eq. 9 represents the statement of macroscopic electroneutrality in the pore, accounting also for the solid skeleton charge. Using Eq. 4 for the half-spacing, b, the solid charge concentration, $\bar{c}_{sk}$, can be expressed as follows:

$$\bar{c}_{sk} = \frac{\bar{c}_{sk,0}}{e} = \frac{(1-f_{Stem})\sigma}{F}\frac{\rho_{sk}S'}{e}$$

(10)

where:

$\bar{c}_{sk,0} = \frac{(1-f_{Stem})\sigma}{F}\rho_{sk}S'$ = solid skeleton charge concentration referring to the solid volume

$(mol \cdot m^{-3})$;

$f_{Stem} = \frac{\sigma_{Stem}}{\sigma}$ = fraction of electric charge compensated by the cations specifically adsorbed in

the Stern layer (-).

Quirk and Marčelja (1997) reported values of f_{Stern} ranging from 0.68 to 0.80 for Lithium ions, with higher values in correspondence to higher concentrations. Ions like Na^+, K^+ or Ca^{2+}, which have smaller hydrated radii, are expected to be characterized by higher values of f_{Stern}. Dominijanni and Manassero (2010) expressed Eq. 10, introducing the cation exchange capacity, $CEC = \frac{\sigma \cdot S}{F}$, as follows:

$$\bar{c}_{sk} = \frac{\bar{c}_{sk,0}}{e} = \phi_{sk} \cdot CEC \cdot \rho_{sk} \cdot \frac{1}{e}$$

(11)

where

ρ_{sk} = density of the solid phase (kg·m^{-3});

$\phi_{sk} = \dfrac{(1 - f_{Stem}) \cdot S'}{S}$ = solid skeleton charge coefficient (-).

In the DDL theory, the Poisson equation is coupled to the equations that impose the equality between the electro-chemical potentials of the components of the soil solution and the electro-chemical potentials of the components of a virtual bulk solution at the microscopic scale:

$$\overline{\mu}_i^{ec,micro} = \mu_i^{ec} \quad \text{for i = 1, 2, ... , N} \tag{12a}$$

$$\overline{\mu}_w^{micro} = \mu_w \tag{12b}$$

where

$\overline{\mu}_i^{ec,micro} = \mu_i^0 + RT\ln(\overline{c}_i^{micro}) + z_i F\overline{\phi}^{micro}$ = electro-chemical potential of the i-th ion;

$\mu_i^{ec} = \mu_i^0 + RT\ln(c_i) + z_i F\phi$ = electro-chemical potential of the i-th ion in the corresponding virtual bulk solution;

$\overline{\mu}_w^{micro} = \mu_w^0 + \dfrac{(\overline{u}^{micro} - \overline{\Pi}^{micro})}{\overline{c}_w}$ = chemical potential of water;

$\mu_w = \mu_w^0 + \dfrac{(u - \Pi)}{c_w}$ = chemical potential of water in the corresponding virtual bulk solution;

μ_i^0, μ_w^0 = constants of integration;

$\overline{\Pi}^{micro} = RT\sum\limits_{i=1}^{N} \overline{c}_i^{micro}$ = osmotic pressure in the pore solution;

$\Pi = RT\sum\limits_{i=1}^{N} c_i$ = osmotic pressure in the virtual solution;

R = universal gas constant (= 8.314 J·mol^{-1}·K^{-1});

T = absolute temperature.

Using the definitions of electro-chemical potentials, Eqs. 12 may be written as follows:

$$\overline{c}_i^{micro} = c_i \exp\left(-z_i \frac{F}{RT} \overline{\psi}^{micro}\right) \tag{13a}$$

$$\overline{u}^{micro} = u - \Pi + \overline{\Pi} \tag{13b}$$

The ion concentration distribution given by Eq. 13a is known as the Boltzmann distribution., The Poisson-Boltzmann equation is obtained, coupling Eq. 7 with Eq. 13a:

$$\frac{d^2 \overline{\psi}^{micro}}{dy^2} = -\frac{F}{\varepsilon_r \varepsilon_0} \sum_{i=1}^{N} z_i c_i \exp\left(-z_i \frac{F}{RT} \overline{\psi}^{micro}\right). \tag{14}$$

The Poisson-Boltzmann equation must be solved to evaluate macroscopic variables through the DDL theory. However, due to its strong non-linearity, only approximate or numerical solutions can be obtained.

As an alternative, a simplifying hypothesis can be adopted, assuming, as a first approximation, that the microscopic variables can be considered equal to the corresponding macroscopic variables, i.e. $\overline{c}_i^{micro} \cong \left\langle \overline{c}_i^{micro} \right\rangle = \overline{c}_i$, $\overline{u}^{micro} \cong \left\langle \overline{u}^{micro} \right\rangle = \overline{u}$ and $\overline{\varphi}^{micro} \cong \left\langle \overline{\varphi}^{micro} \right\rangle = \overline{\varphi}$. Considering Eqs. 13, this assumption is equivalent to assuming a constant distribution of the electric potential in the pore section.

Equality between the electric-potential can then be imposed directly at the macroscopic scale:

$$\overline{\mu}_i^{ec} = \mu_i^{ec} \quad \text{for } i = 1, 2, \ldots, N \tag{15a}$$

$$\overline{\mu}_w = \mu_w \tag{15b}$$

where

$\bar{\mu}_i^{ec} = \mu_i^0 + RT \ln(\bar{c}_i) + z_i F \bar{\varphi}$ = electro-chemical potential of the i-th ion in the pore solution at the macroscopic scale;

$\bar{\mu}_w = \mu_w^0 + \dfrac{(\bar{u} - \bar{\Pi})}{\bar{c}_w}$ = chemical potential of water in the pore solution at the macroscopic scale;

$\bar{\Pi} = RT \sum\limits_{i=1}^{N} \bar{c}_i$ = osmotic pressure ion in the pore solution at the macroscopic scale.

Eqs. 15 are known as the Donnan equations (Donnan, 1911) and, using the chemical and electro-chemical expressions, they can be written in the following form:

$$\bar{c}_i = c_i \exp\left(- z_i \frac{F}{RT} \bar{\psi} \right) \tag{16a}$$

$$\bar{u} = u - \Pi + \bar{\Pi} \tag{16b}$$

where $\bar{\psi} = \bar{\varphi} - \varphi$.

The macroscopic electric potential $\bar{\psi}$ is known as the Donnan potential or membrane potential and it represents the electric potential associated to the solid skeleton charge.

An ion partition coefficient, Γ_i (-), can conveniently be introduced as follows:

$$\Gamma_i = \frac{\bar{c}_i}{c_i} = \exp\left(- z_i \frac{F}{RT} \bar{\psi} \right) \tag{17}$$

This coefficient accounts for the ability of the solid skeleton to determine a partition effect on the ions in the pore solution. When the partition coefficient is higher than 1, the ions are accumulated by the solid skeleton, whereas when the partition coefficient is lower than one, the ions are partially excluded. The ions are completely excluded when the coefficient is equal

to 0. In the absence of an ion partition effect, the coefficient is equal to one for all the ions and there is no difference between the virtual and real concentration in the porous medium.

The Donnan potential $\overline{\psi}$ is evaluated through Eq. 9 concerning the condition of electroneutrality, and the ion concentrations and the hydraulic pressure can therefore be calculated as functions of the virtual variables and the electric charge concentration of the solid skeleton.

The presented analysis clarifies the relation that exists between the DDL theory and the Donnan macroscopic theory. If the microscopic fluctuation of the variables is small with respect to their average value, the error due to the use of the Donnan equilibrium equation, instead of the Poisson-Boltzmann equation, is also small. Considering Eq. 8b concerning the boundary condition of the Poisson-Boltzmann equation, it can be deduced that such microscopic fluctuations are small when the non-dimensional parameter $Q = \dfrac{F}{RT} \dfrac{\sigma_d \cdot b}{\varepsilon_r \varepsilon_0}$ tends to zero.
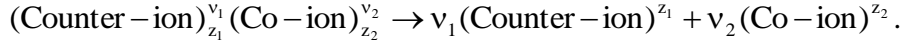
A case of special interest is when the pore solution contains a single salt:

$$(\text{Counter} - \text{ion})_{z_1}^{\nu_1} (\text{Co} - \text{ion})_{z_2}^{\nu_2}$$
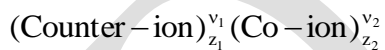
consisting of a counter-ion (charge polarity opposite that of the solid skeleton charge) and a co-ion (same charge polarity as the solid skeleton); (ν_1, z_1) and (ν_2, z_2) are the stoichiometric coefficient and the electrochemical valence of the counter-ion (index 1) and the co-ion (index 2), respectively. Montmorillonite particles have a negative net electric charge: as a result, the counter-ions are the cations (positive charged ion molecules) and the co-ions are the anions (negative charged ion molecules).

The salt in the solution is considered to be completely dissociated on the basis of the following stoichiometric reaction:

$$(\text{Counter}-\text{ion})_{z_1}^{\nu_1}(\text{Co}-\text{ion})_{z_2}^{\nu_2} \rightarrow \nu_1(\text{Counter}-\text{ion})^{z_1} + \nu_2(\text{Co}-\text{ion})^{z_2}.$$

The electroneutrality condition (Eq. 9) can be written as follows:

$$z_1 \cdot \bar{c}_1 + z_2 \cdot \bar{c}_2 = \bar{c}_{sk} \tag{18}$$

where $\bar{c}_1$ and $\bar{c}_2$ represent the cation and anion concentrations, respectively.

Then, introducing the ion partition coefficient, the following equation can be derived:

$$\Gamma_2^{-\nu_2/\nu_1} - \Gamma_2 - \frac{\bar{c}_{sk}}{z_1\nu_1 c_s} = 0. \tag{19}$$

where $c_s = \dfrac{c_1}{\nu_1} = \dfrac{c_2}{\nu_2}$ represents the salt concentration of the corresponding virtual solution.

This latter equation can be solved to relate the partition coefficients to the virtual salt concentration, c_s, and the concentration of the solid skeleton charge, $\bar{c}_{sk}$. Under static conditions, i.e. in the absences of mass fluxes, the virtual solution can be identified with an external bulk solution, which is placed in contact with the porous medium for enough time to reach an equilibrium condition.

An analytical solution can be found for specific cases. For a 1:1 electrolyte (eg. NaCl or KCl) the anion partition coefficient results to be (Katchalsky and Curran, 1965):

$$\Gamma_2 = -\frac{\xi}{2} + \sqrt{\left(\frac{\xi}{2}\right)^2 + 1} \tag{20}$$

where $\xi = \dfrac{\overline{c}_{sk}}{c_s}$;

while for a 2:1 electrolyte (e.g. $CaCl_2$ or $MgCl_2$) it results to be:

$$\Gamma_2 = \frac{2}{3 \cdot \Im(\xi/2)} \left(\frac{\xi}{2}\right)^2 - \frac{1}{3}\left(\frac{\xi}{2}\right) + \frac{1}{6}\Im(\xi/2) \tag{21}$$

where $\Im(\alpha) = \left[108 - 8 \cdot \alpha^3 + 12 \cdot (81 - 12 \cdot \alpha^3)^{1/2}\right]^{1/3}$.

The cation partition coefficient can be obtained from Eq. 17, which gives the following relationship between the ion partition coefficients:

$$\Gamma_1 = \Gamma_2^{-\upsilon_2/\upsilon_1} = \Gamma_2^{-|z_1|/|z_2|} \tag{22}$$

The cation partition coefficient, Γ_1, and the anion partition coefficient, Γ_2, are plotted in Fig. 3a and in Fig. 3b as a function of the normalized salt concentration, $\chi = \xi^{-1} = c_s / \overline{c}_{sk}$, for a solution containing a (1:1) and a (2:1) electrolyte. When the solution contains a (2:1) electrolyte, the partition ability of the bentonite is considerably reduced. It should be noted that Γ_1 is plotted on a logarithmic scale, while Γ_2 is plotted on an arithmetic scale.

The partition coefficients relate the ion concentrations in the bentonite pores to the virtual salt concentration c_s. The partition coefficients describe the ability of the membrane to alter the salt concentration with respect to the external bulk solution. The coefficient $\Gamma_1 \geq 1$ represents the accumulation of the cations, whereas the coefficient $0 \leq \Gamma_2 \leq 1$ indicates the exclusion of

the anions from the pore. When $\Gamma_1 = \Gamma_2 = 1$, the membrane does not generate a partition of the ions and does not have any selective capability; when $\Gamma_2 = 0$ and $\Gamma_1 \to \infty$, the membrane is "ideal" or "perfect", being able to hinder the passage of the salt completely.

TRANSPORT EQUATIONS

According to Gross and Osterle (1968), Cwirko and Carbonell (1988), Yaroshchuk (1995) and Moyne and Murad (2002), the transport equations at the microscopic scale can be expressed by means of the Generalized Nernst-Planck Equations for ion mass transport and the Generalized Navier-Stokes Equation for volumetric liquid transport, provided that the solution can be assumed ideal, i.e. infinitely diluted, and chemical reactions do not occur. These equations may be written in the axial direction as follows:

$$v_x = -\frac{1}{\mu_w} \int_y^b dy' \int_0^{y'} \left(\frac{\partial \overline{u}}{\partial x} - \rho_w g + F \sum_{i=1}^{Nions} z_i \overline{c}_i \frac{\partial \overline{\varphi}}{\partial x} \right) dy''$$ (23a)

$$j_i = v_x \overline{c}_i - D_{i,0} \frac{\partial \overline{c}_i}{\partial x} - z_i \frac{F}{RT} D_{i,0} \overline{c}_i \frac{\partial \overline{\varphi}}{\partial x} \qquad \text{for } i = 1, 2, \dots , N$$ (23b)

where

v_x = liquid velocity in the pore relative to the solid skeleton ($m \cdot s^{-1}$);

j_i = pore flux of the i-th ion relative to the solid skeleton ($mol \cdot m^{-2} \cdot s^{-1}$);

μ_w = water viscosity (= 10^{-3} $Pa \cdot s^{-1}$);

ρ_w = water density (= 1000 $kg \cdot m^{-3}$);

g = gravity acceleration (= 9.81 $m \cdot s^{-2}$);

$D_{i,0}$ = diffusion coefficient in free solution of the i-th ion ($m^2 \cdot s^{-1}$).

Eqs. 23 can be interpreted as the momentum balance equations of the components of the liquid phase. The assumption in Eq. 23b that flux j_i does not depend on the concentration gradient of the other ions that are different from the i-th ion is a consequence of the hypothesis of dilution of the ions in the pore solution: if the i-th ion species is very diluted, it can be expected that it only exchanges momentum with water, i.e. the solvent, and not with

other ion species. Therefore, the coefficient $D_{0,i}$ accounts for the friction between the i-th ion and water. The gravity and electric fields are taken into account in Eqs. 23.

The assumption of an infinitely diluted solution is generally considered reasonable for most geotechenical and geoenvironmental engineering applications that deal with natural soil water and landfill leachate, in which the ion concentrations are expected to be relatively low (Bear, 1972; Freeze and Cherry, 1979). Chemical reactions have not been considered in the present treatment, but they can be taken into account for specific problems by adding a source/sink term.

Coupling transport Eqs. 23 with Poisson-Boltzmann Eq. 7 allows an analysis to be made of electrolyte solution transport through the porous medium in the single pore. Such a set of equations is known in literature as the space-charge model. Due to the non-linearity of the Poisson-Boltzmann equation, only numerical solutions can be provided for such a set of equations.

An approximate solution can be evaluated if the microscopic fluctuations of the variables are neglected with respect to their average values, in a similar manner to what is assumed in Donnas's equations. Then, taking $\overline{c}_i^{micro} \cong \left\langle \overline{c}_i^{micro} \right\rangle = \overline{c}_i$, $\overline{u}^{micro} \cong \left\langle \overline{u}^{micro} \right\rangle = \overline{u}$ and $\overline{\phi}^{micro} \cong \left\langle \overline{\phi}^{micro} \right\rangle = \overline{\phi}$, as a first approximation, the following macroscopic equations can be obtained from Eqs. 23:

$$q = n\tau_m \left\langle v_x \right\rangle = -\frac{k_\phi}{\gamma_w}\left(\frac{\partial \overline{u}}{\partial x} - \rho_w g + F\sum_{i=1}^{N} z_i \overline{c}_i \frac{\partial \overline{\phi}}{\partial x} \right) \tag{24a}$$

$$J_i = n\tau_m \left\langle j_i \right\rangle = q\overline{c}_i - nD_i^* \frac{\partial \overline{c}_i}{\partial x} - nz_i \frac{F}{RT}D_i^* \overline{c}_i \frac{\partial \overline{\phi}}{\partial x} \qquad \text{for i = 1, 2, ... , N} \tag{24b}$$

where

τ_m = non-dimensional matrix tortuosity factor that accounts for the tortuous nature of the actual diffusive pathways through the porous medium due to the geometry of the interconnected pores (<1);

$D_i^* = \tau_m D_{0,i}$ = effective diffusion coefficient of the i-th ion ($m^2 \cdot s^{-1}$);

$k_\phi = n \dfrac{\tau_m}{3 \cdot \mu_w} \gamma_w \dfrac{e^2}{(\rho_s S')^2}$ = hydraulic conductivity at constant electric potential gradient ($m \cdot s^{-1}$).

$\gamma_w = \rho_w \cdot g$ = water weight per unit volume ($\cong 9.81\ kN/m^3$)

Macroscopic Eqs. 24 govern the transport of the electrolyte solution when a homogeneous distribution of the variables is assumed at the microscopic scale. Hydraulic conductivity, k_ϕ, can be expressed through a Kozeny-Carman equation, which accounts for the effective specific surface of bentonite, S'.

Using the identity between the electro-chemical potential at the macroscopic scale (Donnan's equations), Eqs. 24 can be expressed in terms of virtual variables as follows:

$$q = -\frac{k_\phi}{\gamma_w}\left[\left(\frac{\partial u}{\partial x} - \frac{\partial \Pi}{\partial x} - \rho_w g\right) + \sum_{i=1}^{N} \Gamma_i c_i \frac{\partial \mu_i^{ec}}{\partial x}\right] \tag{25a}$$

$$J_i = q \cdot c_i \cdot \Gamma_i - \frac{n D_i^* \Gamma_i}{RT} \frac{\partial \mu_i^{ec}}{\partial x} \qquad \text{for } i = 1, 2, \ldots, N \tag{25b}$$

where

$d\Pi = RT \cdot \sum_{i=1}^{N} c_i$ = osmotic pressure increment of the virtual solution;

$d\mu_i^{ec} = (d\mu_i)_T + z_i F d\varphi$ = electro-chemical potential increment of the i-th ion;

$(d\mu_i)_T = \dfrac{RT}{c_i} dc_i$ = chemical potential increment of the i-th ion at constant temperature.

Eqs. 25 can be compared with the phenomenological equations derived in Dominijanni and Manassero (2011), that can be formulated as follows:

$$q = -\ell_{ww}\left(\frac{\partial u}{\partial x} - \frac{\partial \Pi}{\partial x} - \rho_w g\right) - \sum_{i=1}^{N} \ell_{wi} \frac{\partial \mu_i^{ec}}{\partial x} \tag{26a}$$

$$J_i = -\ell_{iw}\left(\frac{\partial u}{\partial x} - \frac{\partial \Pi}{\partial x} - \rho_w g\right) - \sum_{j=1}^{N} \ell_{ij} \frac{\partial \mu_j^{ec}}{\partial x} \qquad \text{for } i = 1, 2, \dots, N \tag{26b}$$

or in the following alternative way, which is more suitable for an experimental determination of the phenomenological coefficients:

$$q = -\ell_{ww}\left[\left(\frac{\partial u}{\partial x} - \frac{\partial \Pi}{\partial x} - \rho_w g\right) + \sum_{i=1}^{N}(1-\omega_i)\cdot c_i \cdot \frac{\partial \mu_i^{ec}}{\partial x}\right] \tag{27a}$$

$$J_i = (1-\omega_i)\cdot c_i \cdot q - \sum_{j=1}^{N} \tilde{\ell}_{ij} \frac{\partial \mu_j^{ec}}{\partial x} \qquad \text{for } i = 1, 2, \dots, N \tag{27b}$$

where

$\ell_{ww}, \ell_{wi}, \ell_{iw}, \ell_{ij}, \ \omega_i = 1 - \dfrac{1}{c_i}\dfrac{\ell_{iw}}{\ell_{ww}}, \ \tilde{\ell}_{ij} = \ell_{ij} - \dfrac{\ell_{iw}\ell_{jw}}{\ell_{ww}}$ are the phenomenological coefficients.

On the basis of the Onsager's reciprocal relations (Onsager, 1931a,b), the following identities can be inferred:

$$\ell_{wi} = \ell_{iw} \tag{28a}$$

$$\ell_{ij} = \ell_{ji} \qquad \text{for } i \neq j \tag{28b}$$

$$\tilde{\ell}_{ij} = \tilde{\ell}_{ji} \qquad \text{for } i \neq j \tag{28c}$$

for i,j = 1, 2, ... , N.

Then, comparing Eqs. 25 with phenomenological Eqs. 26 and 27, the following physical identification of the phenomenological parameters can be obtained:

$$\ell_{ww} = \frac{k_\phi}{\gamma_w} \tag{29a}$$

$$\ell_{iw} = \frac{k_\phi}{\gamma_w} \Gamma_i c_i \tag{29b}$$

$$\ell_{ii} = n\Gamma_i c_i \frac{D_i^*}{RT} + \frac{k_\phi}{\gamma_w}(\Gamma_i c_i)^2 \tag{29c}$$

$$\ell_{ij} = \frac{k_\phi}{\gamma_w} \Gamma_i c_i \Gamma_j c_j \qquad i \neq j \tag{29d}$$

$$\omega_i = 1 - \Gamma_i \tag{29e}$$

$$\tilde{\ell}_{ii} = n\Gamma_i c_i \frac{D_i^*}{RT} \tag{29f}$$

$$\tilde{\ell}_{ij} = 0 \qquad i \neq j \tag{29g}$$

for i, j = 1,2,…,N.

A physical identification of the phenomenological coefficients is conditioned by the implicit assumptions in Eqs. 23. In particular, the coefficient $\tilde{\ell}_{ij}$ with i ≠ j results to be equal to zero due to the fact that the interactions between the ions are neglected in the Nernst-Planck equations. Onsager's reciprocal relations can be confirmed from the physical interpretation,

when the interactions between the different components of the system are binary. The coupling between the water and ions is closely related to the ion partition effects. When $\Gamma_i = 1$ for all the ions, the osmotic coefficients ω_i result to be null: in such a condition, the classical advective-diffusive transport theory is restored.

For a contaminant transport analysis, the condition of null electrical current has to be added to the previous equations:

$$I_e = F \cdot \left(\sum_{i=1}^{N} z_i J_i \right) = 0 \tag{30}$$

where I_e is the electric current density.

The most interesting case, from an applicative point of view, is that of a solution containing a single salt. Accounting for the condition given by Eq. 30, the following phenomenological equations were derived in Dominijanni and Manassero (2011):

$$q = -\alpha_{ww} \left(\frac{\partial u}{\partial x} - \rho_w g - \omega \frac{\partial \Pi}{\partial x} \right) \tag{31a}$$

$$J_s = (1 - \omega) \cdot q \cdot c_s - P_s \cdot \frac{\partial c_s}{\partial x} \tag{31b}$$

where:

$\omega = -\dfrac{\alpha_{ws}}{\alpha_{ww} c_s}$ = reflection coefficient or chemico-osmotic efficiency coefficient, which is also frequently indicated with the symbol σ in biological and chemical literature (-);

$P_s = \left(\alpha_{ss} - \dfrac{\alpha_{sw}^2}{\alpha_{ww}} \right) \dfrac{RT(\nu_1 + \nu_2)}{c_s}$ = solute permeability ($m^2 \cdot s^{-1}$);

The following identification of the phenomenological parameters used in Eqs.31 can be obtained for this case (Dominijanni, 2005):

$$\alpha_{ww} = \frac{k}{\gamma_w} \qquad (32a)$$

$$\omega = 1 - \frac{\nu_1 D_2^* + \nu_2 D_1^*}{\nu_1 \Gamma_2 D_2^* + \nu_2 \Gamma_1 D_1^*} \Gamma_1 \Gamma_2 \qquad (32b)$$

$$P_s = (1 - \omega) \cdot nD_s^* \qquad (32c)$$

where

$$k = n \frac{\tau_m}{3 \cdot \mu_e} \gamma_w \frac{e^2}{(\rho_s S')^2} = \text{hydraulic conductivity at zero electric current (m·s}^{-1});$$

$$\mu_e = \mu_w + \frac{\tau_m}{3} \frac{e^2}{(\rho_s S')^2} \frac{\bar{c}_{sk}^2 RT}{\sum_{i=1}^{N} z_i^2 D_i^* \bar{c}_i} = \text{electro-viscosity coefficient (Pa·s}^{-1});$$

$$D_s^* = \tau_m \cdot D_{s,0} = \text{salt effective diffusion coefficient (m}^2\text{·s}^{-1});$$

$$D_{s,0} = \frac{(\nu_1 + \nu_2)D_{1,0}D_{2,0}}{\nu_1 D_{2,0} + \nu_2 D_{1,0}} = \frac{(|z_1| + |z_2|)D_{1,0}D_{2,0}}{|z_1|D_{1,0} + |z_2|D_{2,0}} = \text{salt diffusion coefficient in free solution.}$$

Such a physical identification allows the following comments to be made:

1) the hydraulic conductivity at zero electric current, as usually measured in laboratory experiments, can be expressed through a Kozeny-Carman type of equation, in which the water viscosity is substituted by the electro-viscosity coefficient. Such a coefficient accounts for the increase in water viscosity due to the accumulation of cations in the pore;

2) the reflection coefficient accounts for the osmotic phenomenon and results to be null when $\Gamma_i = 1$ for all the ions. This result points out that the macroscopic osmotic phenomena can be

explained by invoking the ion partition effect at the microscopic scale only. A simpler expression of the coefficient ω can be obtained for a (1:1) electrolyte:

$$\omega = 1 - \frac{2}{\sqrt{\xi^2 + 4} + (2t_1 - 1)\xi}, \tag{33}$$

where:

$$t_1 = \frac{D_{1,0}}{D_{1,0} + D_{2,0}} = \text{transport number of the cation ion (-);}$$

$$\xi = \frac{\overline{c}_{sk}}{c_s}.$$

On the basis of Eq.33, ω can assume negative values in the presence of low values of the transport number of the cation, t_1 (i.e. when the anions have a much greater mobility than the cations) for 1:1 electrolytes. For example the dependency of ω on the value of the cation transport number and the relative salt concentration, $\chi = c_s / \overline{c}_{sk}$, is illustrated for a 1:1 electrolyte in Fig. 4. When t_1 is smaller than 0.5, ω can assume negative values. When the salt concentration increases or the concentration of solid skeleton electric charge, $\overline{c}_{sk}$, decreases, parameter ω decreases.

When the solution contains a 2:1 electrolyte, the restrictive capacity of the membrane is reduced. This phenomenon is clearly illustrated in Fig. 5, where ω is plotted as a function of the relative salt concentration, χ, for the case of KCl and $CaCl_2$ solution.

3) the solute permeability P_s is linearly related to the complement to 1 of ω. This result is a consequence of the physical assumption made in the derivation of the equations and, in

particular, the hypothesis that the microscopic fluctuations of the variables can be neglected with respect to their average values. When $\omega = 0$, the solute permeability is equal to the product of the porosity times the effective diffusion coefficient of the salt, and the classical advective-diffusive transport theory is therefore restored. When $\omega = 1$, the solute permeability is null and the salt flux is also null. Therefore, the condition $\omega = 1$ is sufficient to identify a "perfect" or "ideal" membrane, that is able to completely hinder the passage of the salt.

PORO-ELASTIC CONSTITUTIVE EQUATIONS

In soil mechanics, macroscopic strains are related to effective stresses, which are defined as the difference between the total stresses and the pore water pressure (Terzaghi, 1925). The effective stress principle, for a charged porous medium, such as bentonite, can be expressed as follows:

$$\sigma' = \sigma - \bar{u} \tag{34}$$

where

σ' = effective stress (Pa);

σ = total stress (Pa).

The effective stress can be interpreted as the intergranular stress, which is transmitted through ideal springs that link the solid particles (Fig. 6). The springs represent the intergranular contacts between the solid particles, whose real geometry is not constituted by perfectly horizontal platelets. This identification is based on the assumption that the area of the intergranular contacts is very small compared to the total area of a generic section crossing the soil (Skempton, 1961). Under such an assumption, the intergranular stress is defined directly at the macroscopic scale, without having to pass through an upscale procedure.

The pore solution pressure, $\bar{u}$, can be related to the ion concentrations and the concentration of the charge of the solid particles through Donnan's Eq. 16b. It should be stressed that, due the dependency of $\bar{c}_{sk}$ on the void ratio, the pore solution pressure results to be related to the deformation of the bentonite.

Using Eq.16b, the effective stress principle can be formulated as follows:

$$\sigma' = \sigma'_{app} - u_{sw} \tag{35}$$

where

$\sigma'_{app} = \sigma - u$ = apparent effective stress, evaluated with respect to the pressure of the external

bulk solution in equilibrium with the bentonite (Pa);

$u_{sw} = \overline{\overline{\Pi}} - \Pi$ = swelling pressure, which depends on the ion concentration and bentonite void

ratio (Pa).

The concentration of the charge of the solid particles, for uncharged porous media, is equal to

zero (i.e. $\overline{c}_{sk} = 0$), which implies that the ion partition coefficients are equal to unity, and the

osmotic pressure with the bentonite, $\overline{\overline{\Pi}}$, is equal to the osmotic pressure of the virtual

external bulk solution, Π. Therefore, for an uncharged porous medium the swelling pressure,

u_{sw}, is equal to zero and the effective stress, σ', coincides with the apparent effective stress,

σ'_{app}.

The effective stress principle states that the porous medium strains, $d\varepsilon$, are determined by the

effective stress, i.e.

$$d\varepsilon = m_{intergr} \cdot d\sigma' \tag{36}$$

where

$m_{intergr}$ = unidimensional compressibility of the intergranular contacts (Pa^{-1}).

$m_{intergr}$ represents the compressibility of the ideal springs that link the solid particles and

should not be mistaken for the compressibility of the solid particles, which is assumed to be

nil.

It should be stressed that, for the proposed idealized mechanical model, intergranular stress

and strain are evaluated directly at the macroscopic scale, although they have a microscopic

representation. Eq. 36 cannot be considered as the upscaled constitutive equation of a microscopic model, but instead represents a macroscopic relation that is derived from a simplified mechanistic model that represents the soil microstructure.

In the case of elastic behaviour of the solid skeleton, the constitutive equations can be developed as follows for the particular case of a pore solution containing a single salt only:

$$d\varepsilon = m_{intergr} \cdot \left[d\sigma - (du - d\Pi) - d\overline{\overline{\Pi}} \right] = m_{intergr} \cdot \left[d\sigma - (du - d\Pi) - \left(\frac{d\overline{\overline{\Pi}}}{de} de + \frac{d\overline{\overline{\Pi}}}{dc_s} dc_s \right) \right] \quad (37)$$

Observing that $d\varepsilon = -\dfrac{de}{1+e_0}$, Eq. 37 can be expressed as follows:

$$d\varepsilon = \frac{m_{intergr}}{1 - m_{intergr} \dfrac{d\overline{\overline{\Pi}}}{de}(1+e_0)} \cdot \left[d\sigma - (du - d\Pi) - \frac{d\overline{\overline{\Pi}}}{dc_s} dc_s \right] \quad (38)$$

Eq. 38 can be compared with the phenomenological equation derived by Dominijanni and Manassero (2011):

$$d\varepsilon = \beta_{vv} \cdot \left[d\sigma - (du - d\Pi) \right] + \beta_{vs} \cdot (d\mu_s)_T \quad (39)$$

where $(d\mu_s)_T = \dfrac{d\Pi}{c_s}$ is the chemical potential increment of the salt at constant temperature.

Comparing Eq. 38 with phenomenological Eq. 39, the following identification is obtained:

$$\beta_{vv} = \frac{m_{intergr}}{1 - m_{intergr} \dfrac{d\overline{\Pi}}{de}(1 + e_0)} \tag{40a}$$

$$\beta_{vs} = -\frac{m_{intergr}}{1 - m_{intergr} \dfrac{d\overline{\overline{\Pi}}}{de}(1 + e_0)} \frac{d\overline{\Pi}}{dc_s} \frac{c_s}{RT(\nu_1 + \nu_2)} \tag{40b}$$

In the case of a solution containing monovalent ions, the derivatives of osmotic pressure, $\overline{\Pi}$, can be expressed as follows:

$$\frac{d\overline{\Pi}}{de} = -2RT \frac{\overline{c}_{sk,0}^2}{4c_s e^3} \frac{1}{\sqrt{\dfrac{\overline{c}_{sk,0}^2}{4c_s^2 e^2} + 1}} \tag{41a}$$

$$\frac{d\overline{\Pi}}{dc_s} = 2RT \sqrt{\frac{\overline{c}_{sk,0}^2}{4c_s^2 e^2} + 1} - 2RT \frac{\overline{c}_{sk,0}^2}{4e^2 c_s^2} \frac{1}{\sqrt{\dfrac{\overline{c}_{sk,0}^2}{4c_s^2 e^2} + 1}} \tag{41b}$$

Similarly, the real ion concentrations can be expressed as follows:

$$\frac{1}{\nu_1 + \nu_2} d\left[\frac{e}{1 + e_0} \cdot (\overline{c}_1 + \overline{c}_2)\right] = \frac{1}{\nu_1 + \nu_2} d\left[\frac{e}{1 + e_0} \cdot \frac{\overline{\Pi}}{RT}\right] =$$
$$= \frac{1}{(\nu_1 + \nu_2)(1 + e_0)RT}\left(de \cdot \overline{\Pi} + e \cdot \frac{d\overline{\Pi}}{de} de + e \cdot \frac{d\overline{\Pi}}{dc_s} dc_s\right) \tag{42}$$

Using Eq. 38, the following equation is obtained:

$$\frac{1}{\nu_1 + \nu_2} d\left[\frac{e}{1+e_0} \cdot (\overline{c}_1 + \overline{c}_2)\right] =$$

$$= -\frac{1}{(\nu_1 + \nu_2)RT}\left(\overline{\Pi} + e \cdot \frac{d\overline{\overline{\Pi}}}{de}\right) \frac{m_{intergr}}{1 - m_{intergr}\frac{d\overline{\overline{\Pi}}}{de}(1+e_0)} \cdot [d\sigma - (du - d\Pi)] + \tag{43}$$

$$+ \left[\frac{1}{(\nu_1 + \nu_2)RT}\left(\overline{\Pi} + e \cdot \frac{d\overline{\overline{\Pi}}}{de}\right) \frac{m_{intergr}}{1 - m_{intergr}\frac{d\overline{\overline{\Pi}}}{de}(1+e_0)} + \frac{e}{(\nu_1 + \nu_2)(1+e_0)RT}\right] \frac{d\overline{\overline{\Pi}}}{dc_s} dc_s$$

Eq. 43 can be compared with the phenomenological equation derived by Dominijanni and Manassero (2011):

$$\frac{d[e \cdot (\overline{c}_1 + \overline{c}_2)]}{(\nu_1 + \nu_2)(1+e_0)} = \beta_{sv}[d\sigma - (du - d\Pi)] + \beta_{ss} \cdot (d\mu_s)_T \tag{44}$$

From such a comparison, the following identification of the phenomenological coefficients is obtained:

$$\beta_{sv} = -\frac{1}{(\nu_1 + \nu_2)RT}\left(\overline{\Pi} + e \cdot \frac{d\overline{\overline{\Pi}}}{de}\right) \frac{m_{intergr}}{1 - m_{intergr}\frac{d\overline{\overline{\Pi}}}{de}(1+e_0)} \tag{45a}$$

$$\beta_{ss} = \left[\frac{m_{intergr}(1+e_0)\overline{\Pi} + e}{\left[1 - m_{intergr}\frac{d\overline{\overline{\Pi}}}{de}(1+e_0)\right](\nu_1 + \nu_2)RT(1+e_0)}\right] \frac{d\overline{\overline{\Pi}}}{dc_s} \frac{c_s}{RT(\nu_1 + \nu_2)} \tag{45b}$$

Observing that (for a demonstration see Appendix A):

$$\overline{\Pi} + e \cdot \frac{d\overline{\Pi}}{de} = c_s \frac{d\overline{\Pi}}{dc_s} \qquad (46)$$

the reciprocal relation $\beta_{vs} = \beta_{sv}$ is verified for the adopted physical approach.

In bentonite characterized by a very high void ratio, as in suspensions, it can be assumed that there are no contacts between the solid particles, therefore the effective stresses can be considered null. Such an assumption has been made, for instance, by Bolt (1956) and is equivalent to assuming $d\sigma' = 0$ or $m_{intergr} \to \infty$.

As far as the well known mechanical model used by Terzaghi to explain effective stresses in soils (Fig. 7a) is concerned, a simple modification is sufficient to explain the mechanical behaviour of a charged porous medium, such as bentonite. In order to account for the swelling pressure, it is sufficient to add a spring that represents the repulsive forces exchanged by the solid particles at the microscopic scale (see Fig. 7b). From Fig.7b, it is clear that equilibrium with external forces can also be reached in the absence of the spring representing the intergranular contacts.

The dependency of the swelling pressure on the salt concentration of the external bulk solution in equilibrium with bentonite, and the concentration of the charge of solid particles can be appreciated looking at Fig. 8. The swelling pressure is plotted in Fig. 8a as a function of the void ratio, e, and the relative concentration, $c_s / \overline{c}_{sk,0}$, for a 1:1 electrolyte (e.g. NaCl or KCl). The swelling pressure increases when the void ratio, e, and the salt concentration, c_s, decrease, and the reference concentration of the charge of solid particles, $\overline{c}_{sk,0}$, increases. The same swelling pressure behaviour can be appreciated in Fig. 8b for a 2:1 electrolyte (e.g. $CaCl_2$ or $MgCl_2$). From a comparison of Fig. 8a and Fig. 8b, it can be observed that the swelling pressure of a 1:1 electrolyte is always higher than that of a 2:1 electrolyte, under the same conditions.

An interesting development concerns Eq. 39, which can be re-formulated as follows:

$$d\varepsilon = \beta_{vv} \cdot \left(d\sigma - du - du_{sw} \right) \tag{47}$$

where du_{sw} is the increment in the swelling pressure, which is given by:

$$du_{sw} = -\varpi \cdot d\Pi \tag{48}$$

where $\varpi = 1 + \dfrac{\beta_{vs}}{\beta_{vv} \cdot c_s}$ is the swelling pressure coefficient.

It is known, from experimental observations, that the swelling pressure tends to zero when $c_s \to \infty$; therefore the swelling pressure u_{sw} can be obtained as follows:

$$u_{sw} = \int_{\Pi}^{\infty} \varpi \cdot d\Pi \, . \tag{49}$$

Eq. 47 was derived in Dominijanni and Manassero (2011) and it can be considered as a re-formulation of the Terzaghi effective stress principle for charged soils. The effective stresses, in fact, can be identified with the term on the right hand side of Eq. 47, i.e.

$$d\sigma' = d\sigma - du - du_{sw} \tag{50}$$

Terzaghi's classical definition of effective stress is restored when $du_{sw} = 0$, i.e. $\beta_{vs} = 0$: in such a case, the macroscopic compressibility β_{vv} coincide with the compressibility of the intergranular contacts between the solid particles.

Using Eqs. 40, the swelling pressure coefficient ϖ results to be given by:

$$\varpi = 1 - \frac{d\overline{\overline{\Pi}}}{dc_s} \frac{1}{(\nu_1 + \nu_2)RT}. \tag{51}$$

A very interesting finding of the proposed physical model is that ϖ results to be equal to the reflection coefficient ω, when $D_{1,0} = D_{2,0}$. A demonstration of this equality is reported in Appendix B. Moreover, unlike ω, which can assume negative values, ϖ is restricted to vary between 0 and 1, so that it appears to be a better candidate to represent an efficiency coefficient. In particular, ϖ is equal to zero when $\beta_{vs} = 0$, which is the condition that is encountered when $c_s / \overline{c}_{sk} \to \infty$ and $\Gamma_1, \Gamma_2 \to 1$. On the other hand, ϖ is equal to 1 when $c_s / \overline{c}_{sk} \to 0$, so that $\Gamma_1 \to \infty$ and $\Gamma_2 \to 0$.

The equality between ϖ and ω (when $D_{1,0} = D_{2,0}$) is a very interesting result of the physical model, because it allows a transport parameter (ω) to be related to a mechanical parameter (ϖ), in such a way that is possible to obtain information on the mechanical behaviour through the measurement of a transport property and vice versa.

INTERPRETATION OF THE MALUSIS AND SHACKELFORD (2002a,b) EXPERIMENTAL DATA

In order to apply the proposed physical model to the interpretation of experimental tests, the results obtained by Malusis and Shackelford (2002a,b), on samples of a geosynthetic clay liner (GCL) containing bentonite, are interpreted using the relations derived in the previous sections.

Malusis and Shackelford (2002a,b) determined the transport parameters (α_{ww}, ω, P_s) on GCL samples using the testing apparatus described in Malusis et al. (2001). This apparatus consists of a rigid wall cell in which a saturated sample of GCL can be contained. The sample is confined, at the top and the bottom boundaries, by two porous stones in which a continuous circulation of a testing solution can be maintained. A KCl solution has been adopted in the considered tests to represent the potentially polluted leachate produced in a landfill.

Maintaining constant and equal boundary salt concentrations, the hydraulic conductivity, $k = \alpha_{ww} \cdot \gamma_w$, is measured by imposing a hydraulic pressure difference across the sample under steady state conditions, so that:

$$k = \alpha_{ww} \cdot \gamma_w = \gamma_w \cdot \left(\frac{q}{\Delta u} \right)_{\Delta c_s = 0},$$
(52)

where $\Delta u = u' - u''$ represents the difference between the hydraulic pressure at the boundaries of the clay sample and u' and u'' are the values of the hydraulic pressure at the top and the bottom of tha sample, respectively.

The condition of null volumetric flux across the sample ($q = 0$) is imposed to measure ω and P_s, maintaining constant salt concentration values at the sample boundaries. Indicating the salt

concentrations at the top and the bottom of the sample with $c_s{}'$ and $c_s{}''$, respectively, the salt concentration difference is given by:

$$\Delta c_s = c_s{}' - c_s{}''. \tag{53}$$

Malusis and Shackelford (2002a,b) circulated de-ionized water at the bottom of their samples, so that $c_s{}'' = 0$, and assumed the top concentration (i.e. $c_s{}'$) as the reference concentration, c_0 (i.e. $c_0 = c_s{}' = \Delta c_s$).

It is not possible to determine ω and P_s directly because these parameters depend on the salt concentration, which varies across the sample. Only the global or averaged parameters, defined as follows (Auclair et al., 2002):

$$\omega_g = \frac{1}{\Delta c_s} \int_{c_s{}'}^{c_s{}''} \omega \cdot dc_s \tag{54a}$$

$$P_{sg} = \frac{1}{\Delta c_s} \int_{c_s{}'}^{c_s{}''} P_s \cdot dc_s \,, \tag{54b}$$

can be determined from the tests.

It is interesting to observe that the relationship between P_s and ω is also maintained between their corresponding global values: in fact, inserting Eq. 32c into Eq. 54b gives:

$$P_{sg} = (1 - \omega_g) \cdot n \cdot D_s^*. \tag{55}$$

The global parameters ω_g and P_{sg} are determined under steady state conditions as follows:

$$\omega_g = \left(\frac{\Delta u}{\Delta \Pi}\right)_{q=0} \tag{56a}$$

$$P_{sg} = L\left(\frac{J_s}{\Delta c_s}\right)_{q=0} \tag{56b}$$

where L (m) is the length of the sample.

The interpretation of the phenomenological parameters measured by Malusis and Shackelford (2002a,b) is reported in Figs. 9-11. The hydraulic conductivity is plotted in Fig. 9 for a sample with porosity n = 0.79, for different values of the KCl concentration. The reflection coefficient in Fig. 10 is determined for different values of porosity, varying from n = 0.74 to n = 0.86, and for different values of the KCl reference concentration. The solute permeability is reported in Fig. 11 for a sample with porosity n = 0.79, at different values of the KCl reference concentration.

The data relative to the reflection coefficient, ω, have been interpreted using the solid skeleton charge concentration per unit pore volume, $\bar{c}_{sk,0}$, as the only fitting parameter. The theoretical curves are obtained by inserting Eq. 33 into the integral of Eq. 54a, which results in:

$$\omega_g = 1 + \frac{\bar{c}_{sk,0}}{2 \cdot \Delta c_s \cdot e}\left[Z_2 - Z_1 - (2t_1 - 1) \cdot \ln\left(\frac{Z_2 + 2t_1 - 1}{Z_1 + 2t_1 - 1}\right)\right] \tag{57}$$

where $Z_1 = \sqrt{1 + \left(\frac{2 \cdot c_s' \cdot e}{\bar{c}_{sk,0}}\right)^2}$ and $Z_1 = \sqrt{1 + \left(\frac{2 \cdot c_s'' \cdot e}{\bar{c}_{sk,0}}\right)^2}$.

The only undetermined parameter in Eq. 57 is $\bar{c}_{sk,0}$, because the void index, e = n/(1-n), is given for each sample, the boundary salt concentrations are imposed in the test, and the cation

transport number is a function of Potassium and Chloride free solution diffusion coefficients ($D_{K,0} = 19.6 \cdot 10^{-10}$ m^2/s; $D_{Cl,0} = 20.3 \cdot 10^{-10}$ m^2/s; $t_1 = 0.49$).

A value of $\bar{c}_{sk,0}$ equal to 0.464 M has been found from the fitting of the experimental data (Fig. 10). As is possible to see in Fig. 10, the assumption of a constant value for $\bar{c}_{sk,0}$ allows the experimental data to be simulated with an acceptable degree of approximation, when the porosity and salt concentrations vary in the range investigated in the Malusis and Shackelford (2002a,b) tests.

A second physical parameter that can be determined from the theoretical interpretation of the experimental data is the tortuosity factor, τ_m. The most direct way of obtaining this factor is to plot the measured values of P_{sg} as functions of the corresponding values of the complement to 1 of ω_g, i.e. $(1 - \omega_g)$. A linear relationship should be found between these data on the basis of the theoretical model (see Eq. 55). The plot in this graph of the Malusis and Shackleford (2002a,b) data is reported in Fig. 12 together with the theoretical linear relationship. The value of the tortuosity factor is thus obtained from the intercept of the linear function with the ordinate axis at $(1 - \omega_g) = 1$, i.e. $\omega_g = 0$. In fact, the tortuosity factor in Eq. 55, is given by:

$$\tau_m = \left(\frac{P_{sg}}{n \cdot D_{s,0}} \right)_{\omega_g = 0} \tag{58}$$

where $D_{s,0}$ is the KCl free solution diffusion coefficient ($= 19.9 \cdot 10^{-10}$ m^2/s).

A value of τ_m equal to 0.14 has been obtained from the data plotted in Fig. 12. Once τ_m is known, P_{sg} can be calculated for different salt concentration values using Eqs. 55 and 57 (Fig. 11).

The linearity of data reported in Fig. 12 is a validation of the physical model, since Eq. 55 has been derived adopting a number of assumptions and simplifications, the most important of which is that the dispersive phenomena, due to the pore-scale variation of the hydraulic pressure, ion concentrations and water velocity, have been considered negligible. Looking at the data in Fig. 12, it is possible to observe that the linear relationship is in good agreement with the experimental data, thus showing the acceptability of the assumptions made to develop the model.

Once $\bar{c}_{sk,0}$ and τ_m have been determined, the effective specific surface, S', can be evaluated from the hydraulic conductivity data (Fig. 9). The theoretical curve in Fig. 9 has been obtained for a value of S' equal to 127 m^2/g, which means a number of lamellae per tactoid N_l = 6, for a total specific surface S = 760 m^2/g. The electroviscous effect causes a variation in the theoretical hydraulic conductivity as a function of the salt concentration (see Fig. 9) which is close to the level of accuracy of the experimental measure and thus is not very significant. Therefore, as a first approximation, the hydraulic conductivity can be considered constant and equal to the average value, k_{avg} = 1.63·10^{-11} m/s. These conclusions only refer to salt concentration values of c_0 < 1 M. Changes in the bentonite microscopic structure can in fact occur for higher values of salt concentration, and can lead to a reduction in the effective specific surface and, consequently, an increase in the hydraulic conductivity.

One of the most interesting results of the physical model is the equality between the reflection coefficient, ω, and the swelling pressure coefficient, ϖ, when the ion diffusion coefficients are equal to each other. In the case of the KCl solution, the Potassium free solution coefficient ($D_{K,0}$ = 19.6·10^{-10} m^2/s) is practically equal to the Chloride free solution diffusion coefficient ($D_{Cl,0}$ = 20.3·10^{-10} m^2/s), therefore ω can be considered equal to ϖ. As a result, starting from the results of the test for the measurement of the transport parameter, ω, it is possible to evaluate the swelling pressure as a function of the salt concentration and soil porosity. Using

such a theoretical result, the swelling pressure values have been calculated at T = 293 K for the salt concentration and soil porosity ranges investigated by Malusis and Shackelford (2002a,b) (Fig. 13). The theoretical curves in Fig. 13 show the influence of soil porosity, i.e. confinement stress, on the swelling pressure. Moreover, the loss in swelling ability at higher salt concentrations than 0.1 M can be appreciated.

Therefore, on the basis of the physical model, it is possible to obtain information on the mechanical behaviour of bentonite from the results of tests carried out to determine transport parameters. This example highlights the potential usefulness of the theoretical analysis to interpret experimental results, in order to extract the maximum possible amount of information on the behaviour of bentonite.

The experimental results of Malusis and Shackelford (2002a,b) and their theoretical interpretations show that coupled phenomena related to both transport properties and mechanical properties are significant in the presence of dilute salt solutions ($c_0 < 1$ M) or high confinement stresses (corresponding to lower porosity values that have been investigated). When salt concentrations are increased, or in the presence of cation exchange phenomena with divalent ions, such as Calcium, coupled phenomena become less influential on the behaviour of bentonite, which is instead dominated by variations in the microscopic structure, that are determined by montmorillonite lamellae aggregation.

CONCLUSIONS

It could be useful to highlight the limits and potentialities of the proposed physical model. First of all, the assumptions adopted in the theoretical derivation are here pointed out:

1. unidimensional geometry;

2. infinitesimal strains of the solid skeleton;

3. saturated porous medium;

4. incompressible solid and liquid phase;

5. infinitely diluted electrolyte solution;

6. complete dissociation of the salts in the solution;

7. absence of chemical reactions.

The model does not predict or explicitly quantify the effects induced by changes in the bentonite structure, i.e. by changes in the number of particles per tactoide, N_l. In addition, the model does not take into account the dispersive effects, i.e. the effects induced by the fluctuations of the state variables at the pore scale. In spite of these limitations and simplifications, the model allows all the phenomenological coefficients to be correlated to the fundamental variables of the system (i.e. void ratio and ion concentrations), through a limited number of physical parameters of the porous medium ($\overline{c}_{sk,0}$, m_{int}, τ_m, S', ρ_s) and the interstitial fluid (μ_w, ρ_w, $D_{i,0}$).

In particular, the model furnishes a relation between the reflection coefficient, ω, and the solute permeability, P_s, considering the influence of the ion partition effect on these parameters. Moreover, the model offers a validation of Onsager's reciprocal relations, which express the symmetry of the transport phenomenological coefficient matrix.

Another result of the model is the equality between the reflection coefficient, ω, and the swelling pressure coefficient, ϖ, when the cation and anion diffusion coefficients are equal. This relation is a consequence of the identification of the swelling pressure with the difference

between the real and the virtual osmotic pressures and it allows the mechanical behaviour of the soil to be evaluated, starting from experimental data relative to a transport parameter.

The physical approach in general allows correlations between the phenomenological coefficients to be determined, thus reducing the number of tests necessary for soil characterization. In this way, it is possible to extract a large amount of information from a limited number of experimental test results and simulate the expected behaviour in engineering applications.

It should be stressed that the physical model represents a simplified picture of the real soil microstructure, and a direct measurement of its properties at the microscopic scale could be very difficult. For instance, experimental techniques for the direct determination of the effective specific surface or the tortuosity factors are unavailable. The evaluation of the physical properties relies on macroscopic experiments, and the validation of the model is not based on the ability to predict the macroscopic behaviour, but on the capacity to explain the effects produced by changes in the system variables (e.g. ion concentration or soil porosity) on the macroscopic behaviour. The physical approach, even though based on the identification of the phenomena that occur at the microscopic scale, is only aimed at describing the soil behaviour at the macroscopic scale. Therefore, the physical approach should not be mistaken for a microscopic modelling of soil behaviour, but it should be considered as a tool that can be used to help understand why soils behave in a given way at the macroscopic scale on the basis of a simplified picture of their microstructure.

APPENDIX A

The osmotic pressure of pore solution, $\overline{\Pi}$, is given by:

$$\overline{\Pi} = RT \cdot (\overline{c}_1 + \overline{c}_2) \tag{A1}$$

where $\overline{c}_1$ and $\overline{c}_2$ are the cation and anion concentrations, which are related to the virtual salt concentration as follows:

$$c_s = \frac{\overline{c}_1}{\nu_1 \Gamma_1} = \frac{\overline{c}_2}{\nu_2 \Gamma_2}. \tag{A2}$$

Using Eq. A1, $\overline{\Pi}$ can be expressed as a function of c_s and the ion partition coefficients Γ_1 and Γ_2:

$$\overline{\Pi} = RT \cdot c_s \cdot (\nu_1 \Gamma_1 + \nu_2 \Gamma_2) \tag{A3}$$

The ion partition coefficients depend on the salt concentration and the void index through the condition of electroneutrality:

$$z_1 \overline{c}_1 + z_2 \overline{c}_2 = \overline{c}_{sk} \tag{A4}$$

where $\overline{c}_{sk}$ is the solid skeleton charge concentration, referring to the pore volume. Considering Eq. 10, $\overline{c}_{sk}$ is related to the void index, e, through the following relation:

$$\bar{c}_{sk} = \frac{\bar{c}_{sk,0}}{e} \tag{A5}$$

where $\bar{c}_{sk,0}$ is the solid skeleton charge concentration, referring to the solid volume, which, as a first approximation, can be assumed to be independent of c_s and e.

Using Eqs. A2 and A5, the electroneutality condition (Eq. A4) is given by:

$$z_1 v_1 \Gamma_1 + z_2 v_2 \Gamma_2 = \frac{\bar{c}_{sk,0}}{e \cdot c_s} \tag{A6}$$

The electrochemical valences z_1 and z_2 are related to the stoichiometric coefficients v_1 and v_2, through the condition of electroneutrality of the virtual solution:

$$z_1 c_1 + z_2 c_2 = 0 \tag{A7}$$

where the cation and anion concentrations are related to c_s as follows:

$$c_s = \frac{c_1}{v_1} = \frac{c_2}{v_2}. \tag{A8}$$

Substituting Eq. A8 in Eq. A7, the following condition is obtained:

$$z_1 v_1 + z_2 v_2 = 0. \tag{A9}$$

The electroneutrality condition in the porous medium (Eq. A6) can be solved taking into account Eq. A9 and the relation that links the partition coefficients:

$$\Gamma_2 = \Gamma_1^{\frac{z_2}{z_1}} = \Gamma_1^{-\frac{v_2}{v_1}}. \tag{A10}$$

The resulting equation can be expressed taking, for instance, Γ_2 as the variable to find:

$$\Gamma_2^{-\frac{v_2}{v_1}} - \Gamma_2 = \frac{\overline{c}_{sk,0}}{(e \cdot c_s) \cdot z_1 v_1} \tag{A11}$$

It is possible to obtain Γ_2 from the solution of Eq. A11 and then Γ_1 through Eq. A10.

Looking at Eq. A11, it is possible to deduce that the ion partition coefficients, and consequently their weighted sum $v_1\Gamma_1 + v_2\Gamma_2$, can be expressed as a function of the product $(e \cdot c_s)$, i.e.

$$v_1\Gamma_1 + v_2\Gamma_2 = f(e \cdot c_s) \tag{A12}$$

where f represents an unknown function.

As a result, the osmotic pressure of the pore solution, $\overline{\Pi}$, given by Eq. A3 can be expressed in the following form:

$$\overline{\Pi} = RT \cdot c_s \cdot f(e \cdot c_s). \tag{A13}$$

The derivative of $\overline{\Pi}$, with respect to c_s, results to be given by:

$$\frac{d\overline{\Pi}}{dc_s} = RT \cdot f(e \cdot c_s) + RT \cdot c_s \cdot \frac{df(e \cdot c_s)}{dc_s} \tag{A14}$$

where

$$\frac{df(e \cdot c_s)}{dc_s} = \frac{df(e \cdot c_s)}{d(e \cdot c_s)} \cdot \frac{d(e \cdot c_s)}{dc_s} = \frac{df(e \cdot c_s)}{d(e \cdot c_s)} \cdot e. \tag{A15}$$

Proceeding in a similar way, it is possible to obtain an expression for the derivative of $\overline{\Pi}$ with respect to the void index, e:

$$\frac{d\overline{\Pi}}{de} = RT \cdot c_s \cdot \frac{df(e \cdot c_s)}{de} \tag{A16}$$

where

$$\frac{df(e \cdot c_s)}{de} = \frac{df(e \cdot c_s)}{d(e \cdot c_s)} \cdot \frac{d(e \cdot c_s)}{de} = \frac{df(e \cdot c_s)}{d(e \cdot c_s)} \cdot c_s. \tag{A17}$$

Then, using Eq. A14-A17, the following identity is verified:

$$\overline{\Pi} + e \cdot \frac{d\overline{\Pi}}{de} = c_s \frac{d\overline{\Pi}}{dc_s} \tag{A18}$$

which is Eq. 46 in the paper, and it is necessary to prove the equality of the phenomenological coefficients β_{vs} and β_{sv}.

APPENDIX B

The aim of this appendix is to show the equality between the swelling pressure coefficient, ϖ, given by Eq. 51 and the reflection coefficient, ω, when $D_{1,0} = D_{2,0}$.

The reflection coefficient is given by Eq. 32b, which can be expressed in the following form:

$$\omega = 1 - \frac{\nu_1 D_{2,0} + \nu_2 D_{1,0}}{\nu_1 \Gamma_2 D_{2,0} + \nu_2 \Gamma_1 D_{1,0}} \Gamma_1 \Gamma_2 \qquad (B1)$$

if the tortuosity factor $\tau_m = \dfrac{D_1^*}{D_{1,0}} = \dfrac{D_2^*}{D_{2,0}}$ is simplified between the numerator and denominator.

Considering the relationship between the ion partition coefficients given in Eq. A10, ω can only be expressed in terms of Γ_2:

$$\omega = 1 - \frac{\nu_1 D_{2,0} + \nu_2 D_{1,0}}{\nu_1 D_{2,0} \Gamma_2^{\frac{\nu_2}{\nu_1}} + \nu_2 D_{1,0} \Gamma_2^{-1}}. \qquad (B2)$$

When $D_{1,0} = D_{2,0}$ (for instance in the case of a KCl solution, where $D_{K,0} = 19.6 \cdot 10^{-10}$ m^2/s and $D_{Cl,0} = 20.3 \cdot 10^{-10}$ m^2/s), the expression of ω is simplified as follows:

$$\omega = 1 - \frac{\nu_1 + \nu_2}{\nu_1 \Gamma_2^{\frac{\nu_2}{\nu_1}} + \nu_2 \Gamma_2^{-1}}. \qquad (B3)$$

The swelling pressure coefficient ϖ is given by Eq. 51, which is here reported:

$$\varpi = 1 - \frac{d\overline{\Pi}}{dc_s} \frac{1}{(\nu_1 + \nu_2)RT}.$$

(B4)

The aim of the demonstration is to show that Eq. B4 is equal to Eq. B3. In order to obtain this result, we can observe that the derivative of the osmotic pressure of the pore solution, $\overline{\Pi}$, with respect to the virtual salt concentration, c_s, can be obtained by deriving Eq. A3:

$$\frac{d\overline{\Pi}}{dc_s} = RT \cdot (\nu_1 \Gamma_1 + \nu_2 \Gamma_2) + RT \cdot c_s \cdot \left(\nu_1 \frac{d\Gamma_1}{dc_s} + \nu_2 \frac{d\Gamma_2}{dc_s} \right).$$

(B5)

The following relation between the ion partition coefficients can be obtained from Eqs. A6 and A9:

$$\Gamma_1 - \Gamma_2 = \frac{\overline{c}_{sk}}{c_s \cdot z_1 \nu_1}$$

(B6)

where $\overline{c}_{sk} = \dfrac{\overline{c}_{sk,0}}{e}$ is the solid skeleton charge concentration, referring to the pore volume, which only depends on the void index, e.

Deriving Eq. B6, with respect to c_s, it is possible to obtain the derivative of Γ_1 as a function of the derivative of Γ_2 and c_s:

$$\frac{d\Gamma_1}{dc_s} = \frac{d\Gamma_2}{dc_s} - \frac{\overline{c}_{sk}}{c_s^2 \cdot z_1 \nu_1}.$$

(B7)

The derivative of Γ_2 can be obtained by deriving Eq. A11 with respect to c_s:

$$\frac{d}{d\Gamma_2}\left(\Gamma_2^{-\frac{\nu_2}{\nu_1}}\right)\frac{d\Gamma_2}{dc_s} - \frac{d\Gamma_2}{dc_s} = -\frac{\bar{c}_{sk}}{c_s^2 \cdot z_1 \nu_1}. \tag{B8}$$

From Eq. B8, it is possible to obtain $\dfrac{d\Gamma_2}{dc_s}$:

$$\frac{d\Gamma_2}{dc_s} = \frac{\dfrac{\bar{c}_{sk}}{c_s^2 \cdot z_1 \nu_1}}{1 + \dfrac{\nu_2}{\nu_1}\Gamma_2^{-\frac{\nu_2}{\nu_1}-1}}. \tag{B9}$$

If Eq. B7 and B9 are inserted into Eq. B5, the following equation is found for $\dfrac{d\overline{\Pi}}{dc_s}$:

$$\frac{d\overline{\Pi}}{dc_s} = RT \cdot (\nu_1\Gamma_1 + \nu_2\Gamma_2) + RT \cdot c_s \cdot (\nu_1 + \nu_2) \cdot \frac{\dfrac{\bar{c}_{sk}}{c_s^2 \cdot z_1 \nu_1}}{1 + \dfrac{\nu_2}{\nu_1}\Gamma_2^{-\frac{\nu_2}{\nu_1}-1}} - RT \cdot \frac{\bar{c}_{sk}}{z_1 c_s}. \tag{B10}$$

The solid skeleton charge concentration $\bar{c}_{sk}$ can be related to the ion partition coefficients through the condition of electroneutrality within the porous medium (see Eq. A6):

$$\bar{c}_{sk} = (z_1\nu_1\Gamma_1 + z_2\nu_2\Gamma_2) \cdot c_s. \tag{B11}$$

Introducing Eq. B11 into Eq. B10, $\dfrac{d\overline{\Pi}}{dc_s}$ results to be given by:

$$\frac{d\overline{\Pi}}{dc_s} = RT \cdot (\nu_1 + \nu_2) \cdot \left[\Gamma_2 + \frac{\Gamma_2^{-\frac{\nu_2}{\nu_1}} - \Gamma_2}{1 + \frac{\nu_2}{\nu_1} \Gamma_2^{-\frac{\nu_2}{\nu_1} - 1}} \right].$$ (B12)

Multiplying the numerator and denominator in Eq. B12 by $\left(\nu_1 \Gamma_2^{\frac{\nu_2}{\nu_1}} \right)$, the following equation

can be derived:

$$\frac{d\overline{\Pi}}{dc_s} = RT \cdot (\nu_1 + \nu_2) \cdot \left[\frac{\Gamma_2 \cdot \left(\nu_1 \Gamma_2^{\frac{\nu_2}{\nu_1}} + \nu_2 \Gamma_2^{-1} \right) + \left(\Gamma_2^{-\frac{\nu_2}{\nu_1}} - \Gamma_2 \right) \cdot \nu_1 \Gamma_2^{\frac{\nu_2}{\nu_1}}}{\nu_1 \Gamma_2^{\frac{\nu_2}{\nu_1}} + \nu_2 \Gamma_2^{-1}} \right].$$ (B13)

Developing the calculations within the squared brackets in Eq. B13, it is possible to find:

$$\frac{d\overline{\Pi}}{dc_s} = RT \cdot (\nu_1 + \nu_2)^2 \cdot \left(\frac{1}{\nu_1 \Gamma_2^{\frac{\nu_2}{\nu_1}} + \nu_2 \Gamma_2^{-1}} \right).$$ (B14)

Inserting Eq. B14 into Eq. B4, the resulting expression of the swelling coefficient, ϖ, is:

$$\varpi = 1 - \frac{\nu_1 + \nu_2}{\nu_1 \Gamma_2^{\frac{\nu_2}{\nu_1}} + \nu_2 \Gamma_2^{-1}}.$$ (B15)

Comparing Eq. B3 and Eq. B15, the equality between ω and ϖ is obtained, when $D_{1,0} = D_{2,0}$.

REFERENCES

Auclair, B., Nikonenko, V., Larchet, C., Métayer, M., and Dammak, L., 2002. Correlation between transport parameters of ion-exchange membranes. Journal of Membrane Science, 195, 89-102.

Bear, J., 1972. Dynamics of fluids in porous media. American Elsevier, New York, N.Y.

Birgersson, M., and Karnland, O., 2009. Ion equilibrium between montmorillonite interlayer space and an external solution – Consequences for diffusional transport. Geochimica et Cosmochimica Acta, 73, 1908-1923.

Bolt, G.H., 1956. Physico-chemical analysis of the compressibility of pure clays, Géotechnique, 6, 86-93.

Chapman, L., 1913. A contribution to the theory of electrocapillarity, Philosophical Magazine, 25, 475-481.

Coussy, O., 1995. Mechanics of porous continua. John Wiley & Sons, Chichester, England.

Coussy, O., 2004. Poromechanics. John Wiley & Sons, Chichester, England.

Cwirko, E.H., and Carbonell, R.G., 1988. Transport of electrolytes in charged pores: analysis using the method of spatial averaging. Journal of Colloid and Interface Science, 129 (2), 513-531.

Dähnert, K., and Huster, D., 1999. Comparison of the Poisson-Boltzmann model and the Donnan equilibrium of a polyelectrolyte in salt solution. Journal of Colloid and Interface Science, 215, 131-139.

Dominijanni, A., 2005. Osmotic properties of clay soils. PhD Thesis, Politecnico di Torino.

Dominijanni, A., and Manassero, M., 2010. Chemico-osmosis and solute transport through geosynthetic clay liners. In: Geosynthetic clay liners for waste containment, Bouazza A., Bowders J.J. (Eds.), CRC Press, 105-125.

Dominijanni, A., and Manassero, M., 2011. Modelling the swelling and osmotic properties of clay soils: Part I. The phenomenological approach, *submitted for publication*.

Donnan, F.G., 1911. Theorie der Membrangleichgewichte und Membranpotentiale bei Vorhandensein von nicht dialysierenden Elektrolyten. Ein Beitrag zur physikalisch-chemischen Physiologie [Theory of membrane equilibria and membrane potentials in the presence of non-dialysing electrolytes. A contribution to physical-chemical physiology], Zeitschrift für Elektrochemie und angewandte physikalische Chemie, 17, 572-581. English translation republished in Journal of Membrane Science, 100 (1995), 45-55.

Eckart, C., 1940a. The thermodynamics of irreversible processes. I. The simple fluid. Physical Review, 58, 267-269.

Eckart, C., 1940b. The thermodynamics of irreversible processes. II. Fluid mixtures. Physical Review, 58, 269-275.

Freeze, R.A., and Cherry, J.A., 1979. Groundwater, Prentice-Hall, Englewood Cliffs, N.J.

Gouy, G., 1910. Sur la constitution de la charge électrique à la surface d'un electrolyte. Journal de Physique Théorique et Appliquée, 9, 457-468.

Groenevelt, P.H., and Bolt, G.H., 1969. Non-equilibrium thermodynamics of the soil-water system. Journal of Hydrology, 7, 358-388.

Gross, R.J., and Osterle, J.F., 1968. Membrane transport characteristics of ultrafine capillaries. The Journal of Chemical Physics, 49 (1), 228-234.

Guyonnet, D., Gaucher, E., Gaboriau, H., Pons, C.H., Clinard, C., Norotte, V., and Didier, G., 2005. Geosynthetic clay liner interaction with leachate: correlation between permeability, microstructure and surface chemistry, Journal of Geotechnical and Geoenvironmental Engineering, 131 (6), 740-749.

Hanshaw, B.B., and Coplen, T.B., 1973. Ultrafiltration by a compacted clay membrane-II. Sodium ion exclusion at various ionic strengths. Geochimica et Cosmochimica Acta, 37, 2311-2327.

Hoffer, E., and Kedem, O., 1967. Hyperfiltration in charged membranes: the fixed charge model. Desalination, 2, 25-39.

Katchalsky, A., and Curran, P.F., 1965. Nonequilibrium thermodynamics in biophysics. Harvard University Press, Cambridge, MA.

Kedem, O., and Katchalsky, A., 1961. A physical interpretation of the phenomenological coefficients of membrane permeability. Journal of General Physiology, 45, 143-179.

Leroy, P., Revil, A., and Coelho, D., 2006. Diffusion of ionic species in bentonite. Journal of Colloid and Interface Science, 296, 248-255.

Lyklema, J., 2003. Electrokinetics after Smoluchowski. Colloids and Surfaces A: Physicochem. Eng. Aspects, 222, 5-14.

Malusis, M.A., and Shackelford, C.D., 2002a. Chemico-osmotic efficiency of a geosynthetic clay liner. Journal of Geotechnical and Geoenvironmental Engineering, 128(2), 97-106.

Malusis, M.A., and Shackelford, C.D., 2002b. Coupling effects during steady-state solute diffusion through a semi-permeable clay membrane. Environmental Science and Technology, 36, 1312-1319.

Malusis, M.A., Shackelford, C.D., and Olsen, H.W., 2001. A laboratory apparatus to measure chemico-osmotic efficiency coefficients for clay soils. Geotechnical Testing Journal, 24 (3), 229-242.

Marine, I.W., and Fritz, S.J., 1981. Osmotic model to explain anomalous hydraulic heads. Water Resources Research, 17, 73-82.

Meyer, K.H., and Sievers, J.F., 1936a. La perméabilité des membranes I, Théorie de la perméabilité ionique. Helvetica Chimica Acta, 19 (1), 649-664.

Meyer, K.H., and Sievers, J.F., 1936b. La perméabilité des membranes II. Essais avec des membranes sélectives artificielles. Helvetica Chimica Acta, 19 (1), 665-677.

Moyne, C., and Murad, M.A., 2002. Electro-chemo-mechanical couplings in swelling clays derived from a micro/macro-homogenization procedure. International Journal of Solids and Structures, 39, 6159-6190.

Muurinen, A., Karnland, O., and Lehikoinen, J., 2004. Ion concentration caused by an external solution into the porewater of compacted bentonite. Physics and Chemistry of the Earth, 29, 119-127.

Norrish, K., 1954. The swelling of montmorillonite. Discussions of the Faraday Society, 18, 120-134.

Onsager, L., 1931a, Reciprocal relations in irreversible processes I. Physical Review, 37 (4), 405-426.

Onsager, L., 1931b, Reciprocal relations in irreversible processes II. Physical Review, 38 (12), 2265-2279.

Quirk, J.P., and Marčelja, S., 1997. Application of double-layer theories to the extensive crystalline swelling of Li-montmorillonite, Langmuir, 13, 6241-6248.

Revil, A., and Leroy, P., 2004. Constitutive equations for ionic transport in porous shales. Journal of Geophysical Research, 109, B03208, 1-19.

Revil, A., Leroy, P., and Titov, K., 2005. Characterization of transport properties of argillaceous sediments: Application to the Callovo-Oxfordian argillite. Journal of Geophysical Research, 110, B06202, 1-18.

Shainberg, I., Bresler, E., and Klausner, Y., 1971. Studies on Na/Ca montmorillonite systems. 1. The swelling pressure. Soil Science, 111 (4), 214-219.

Skempton, A.W., 1961. Effective stress in soils, concrete and rocks. In Pore pressure and suction in soils, Butterworths, London, 4-16.

Stern, O., 1924. Zur Theorie der elektrischen Doppelschicht. Z. Elektrochem., 30, 508-516.

Teorell, T., 1935. An Attempt to formulate a quantitative theory of membrane permeability. Proceedings of the Society for Experimental Biology and Medicine, 33, 282-283.

Teorell, T., 1937. The properties and functions of membranes, natural and artificial, II Artificial membranes, General discussion. Transactions of the Faraday Society, 33, 1053, 1086-1088.

Terzaghi, K., 1925. Erdbaumechanik auf bodenphysikalische grundlage. Deuticke, Vienna.

Yaroshchuk, A.E., 1995. Osmosis and reverse osmosis in fine-charged diaphragms and membranes. Advances in Colloid and Interface Science, 60, 1-93.
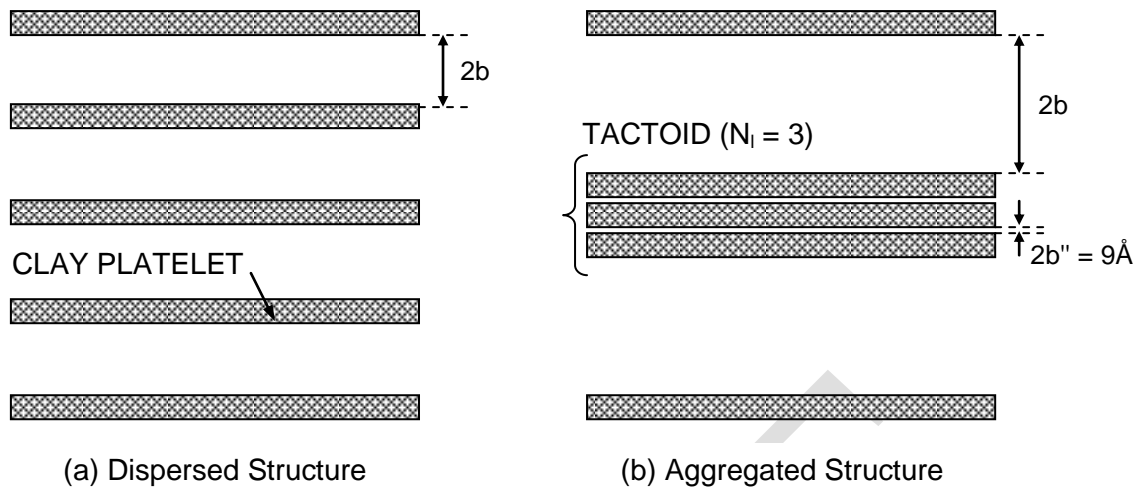
LIST OF FIGURES

Figure No.	Figure Caption
1	Microscopic structure of clay soils containing montmorillonite as the main mineralogical component. The structure can be dispersed (a), if the lamellae of montmorillonite (or clay platelets) are present as individual units, or aggregated (b), if the lamellae are condensed to form the so-called tactoids. Symbols: N_l = number of clay platelets per tactoid; b = half-spacing of the conducting pores; b" = half spacing of the intra-tactoid pores containing immobile water.
2	Slit-like geometry for an idealized bentonite pore. Symbols: x = longitudinal pore axis, corresponding to the macroscopic direction of transport; y = transversal pore axis; L = length of the clay layer; b = half-spacing of the conducting pores; $\overline{\psi}^{micro}$ = electric potential due to the double layer.
3	Cation partition coefficient (a) and anion partition coefficient (b) as a function of the relative salt concentration $\chi = c_s / \overline{c}_{sk}$ for a (1:1) (e.g. NaCl or KCl) and a (2:1) (e.g. $CaCl_2$) electrolyte. It should be noted that Γ_1 is plotted on a logarithmic scale, while Γ_2 is plotted on a arithmetic scale.
4	Reflection coefficient, ω, versus relative salt concentration, $\chi = c_s / \overline{c}_{sk}$, and the cation transport number, $t_1 = D_{1,0}/(D_{1,0}+D_{2,0})$, for a solution containing a (1:1) electrolyte.
5	Reflection coefficient, ω, versus relative salt concentration, $\chi = c_s / \overline{c}_{sk}$, for a solution containing cations with different valences ($z_1 = +1$ for K^+

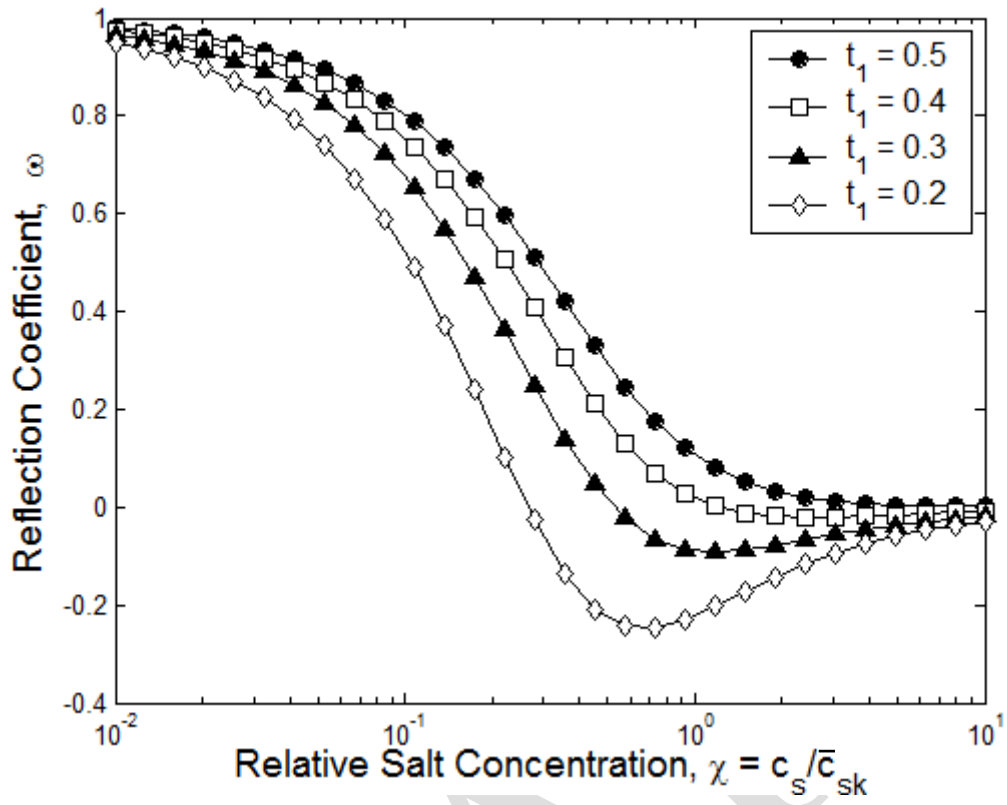|	
	and $z_1 = +2$ for Ca^{2+}).
6	Microscopic idealized mechanical model, where the springs represent the intergranular contacts that transmit the intergranular or effective stress σ'.
7	Mechanical model for (a) an uncharged porous medium and (b) a charged porous medium.
8	Swelling pressure as a function of the void ratio, e, salt concentration, c_s, and charge concentration of the solid particles referring to the solid volume, $\overline{c}_{sk,0}$, for (a) a 1:1 electrolyte and (b) a 2:1 electrolyte.
9	Hydraulic conductivity, k, determined on a GCL sample with porosity n = 0.79 by Malusis and Shackelford (2002a,b) as a function of the KCl reference concentration, c_0, and the theoretical interpretation (continuous line).
10	Global reflection coefficient ω_g measured by Malusis and Shackelford (2002a,b) on GCL samples as a function of the KCl reference concentration, c_0, and soil porosity, n, and the theoretical interpretation (continuous lines).
11	Global solute permeability, P_{sg}, determined on a GCL sample with porosity n = 0.79 by Malusis and Shackelford (2002a,b) as a function of the KCl reference concentration, c_0, and the theoretical interpretation (continuous line).
12	Global solute permeability, P_{sg}, as a function of the complement to 1 of the global reflection coefficient, ω_g, determined on a GCL sample with porosity n = 0.79 by Malusis and Shackelford (2002a,b) and the theoretical linear relationship (continuous line).

13	Theoretical swelling pressure, u_{sw}, as a function of the KCl reference concentration, c_0, and soil porosity, n, for the GCL investigated by Malusis and Shackelford (2002a,b). The theoretical curves have been derived from the equality of the reflection coefficient, ω, and the swelling pressure coefficient, ϖ, for a KCl solution ($D_{K,0} \cong D_{Cl,0}$).

Figure 1. Microscopic structure of clay soils containing montmorillonite as the main mineralogical component. The structure can be dispersed (a), if the lamellae of montmorillonite (or clay platelets) are present as individual units, or aggregated (b), if the lamellae are condensed to form the so-called tactoids. Symbols: N_l = number of clay platelets per tactoid; b = half-spacing of the conducting pores; b'' = half spacing of the intra-tactoid pores containing immobile water.
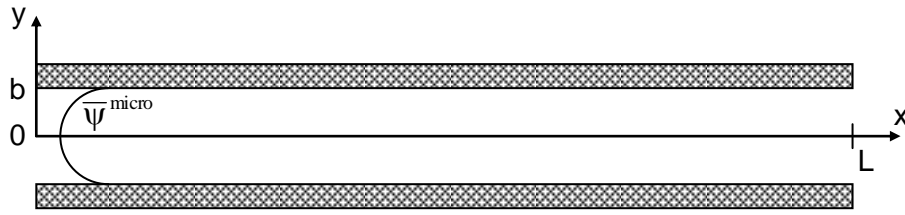
Figure 2. Slit-like geometry for an idealized bentonite pore. Symbols: x = longitudinal pore axis, corresponding to the macroscopic direction of transport; y = transversal pore axis; L = length of the clay layer; b = half-spacing of the conducting pores; $\overline{\psi}^{micro}$ = electric potential due to the double layer.
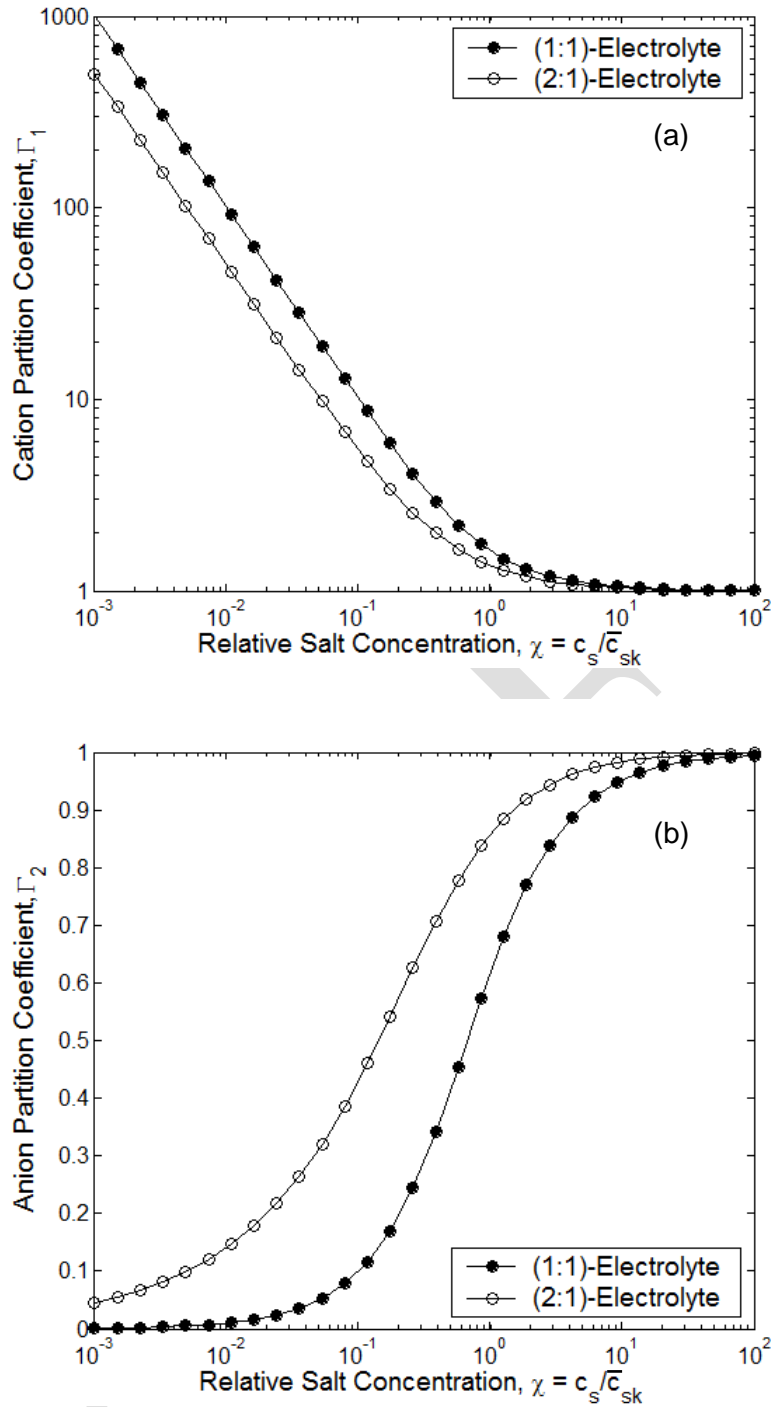
Figure 3. Cation partition coefficient (a) and anion partition coefficient (b) as a function of the relative salt concentration $\chi = c_s / \bar{c}_{sk}$ for a (1:1) (e.g. NaCl or KCl) and a (2:1) (e.g. $CaCl_2$) electrolyte. It should be noted that Γ_1 is plotted on a logarithmic scale, while Γ_2 is plotted on a arithmetic scale.

Figure 4. Reflection coefficient, ω, versus relative salt concentration, $\chi = c_s / \overline{c}_{sk}$, and the cation transport number, $t_1 = D_{1,0}/(D_{1,0}+D_{2,0})$, for a solution containing a (1:1) electrolyte.
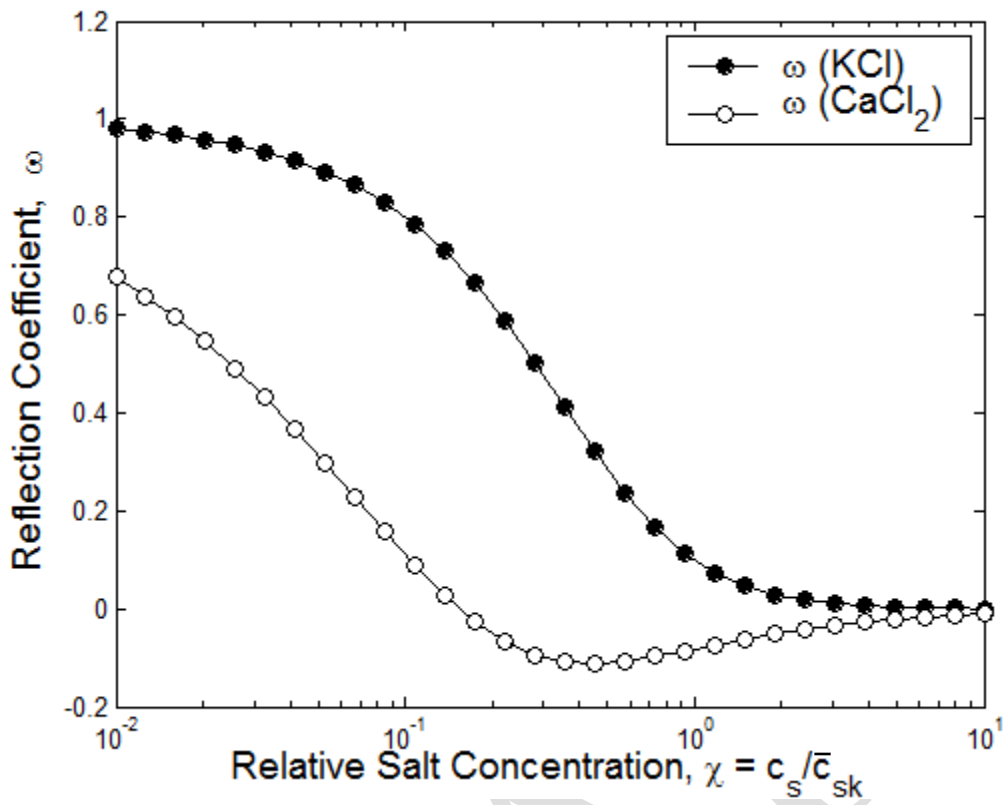
Figure 5. Reflection coefficient, ω, versus relative salt concentration, $\chi = c_s / \bar{c}_{sk}$, for a solution containing cations with different valences ($z_1 = +1$ for K^+ and $z_1 = +2$ for Ca^{2+}).
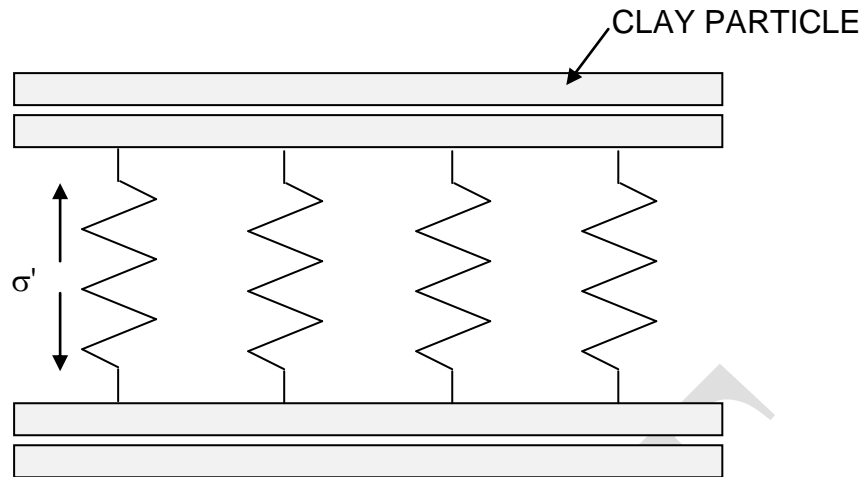
Figure 6. Microscopic idealized mechanical model, where the springs represent the intergranular contacts that transmit the intergranular or effective stress σ'.
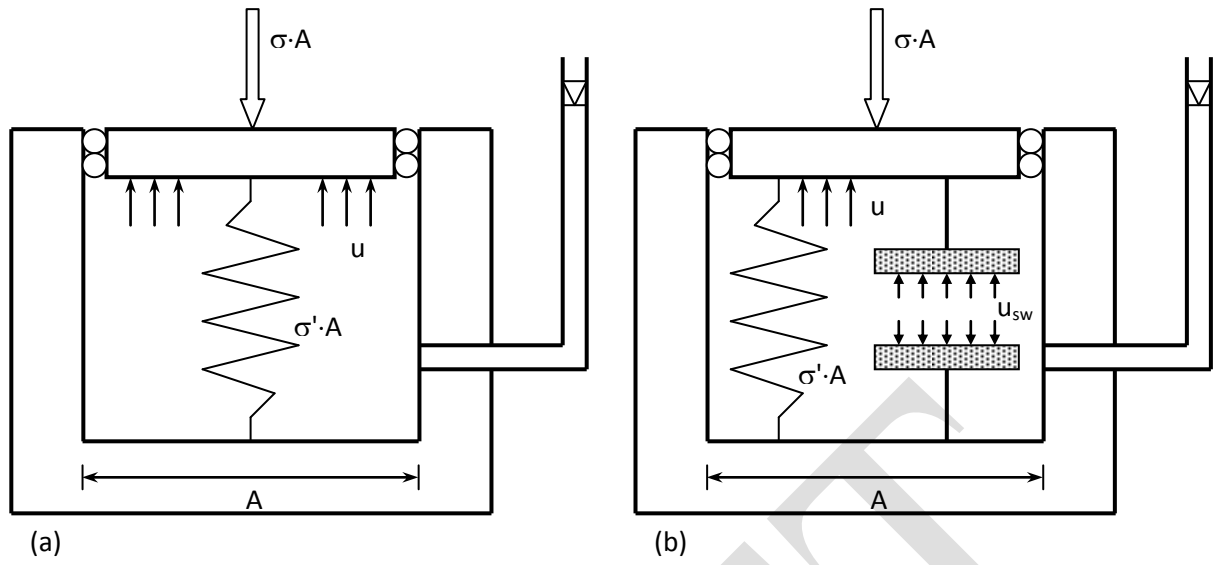
Figure 7. Mechanical model for (a) an uncharged porous medium and (b) a charged porous medium.
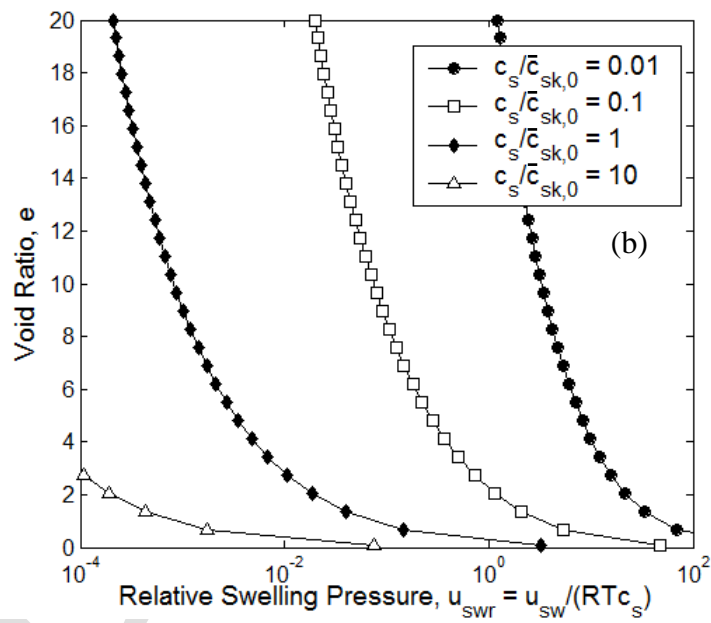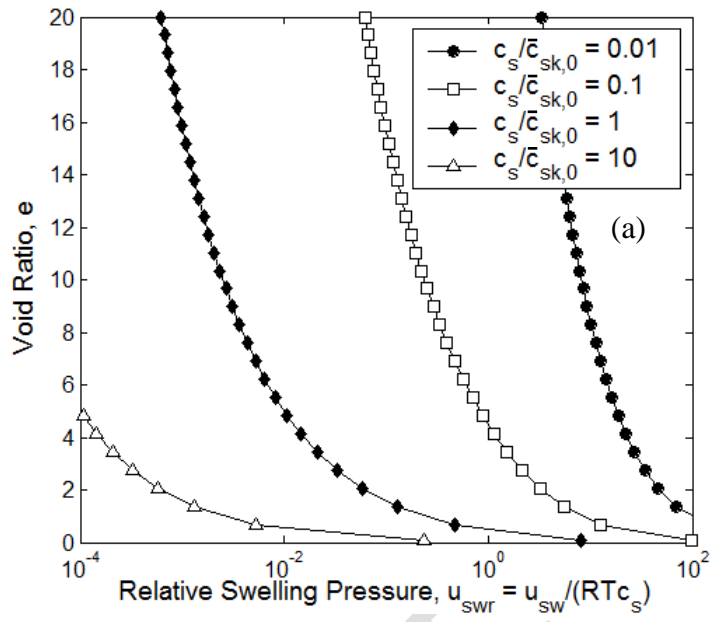
Figure 8. Swelling pressure as a function of the void ratio, e, salt concentration, c_s, and charge concentration of the solid particles referring to the solid volume, $\bar{c}_{sk,0}$, for (a) a 1:1 electrolyte and (b) a 2:1 electrolyte.
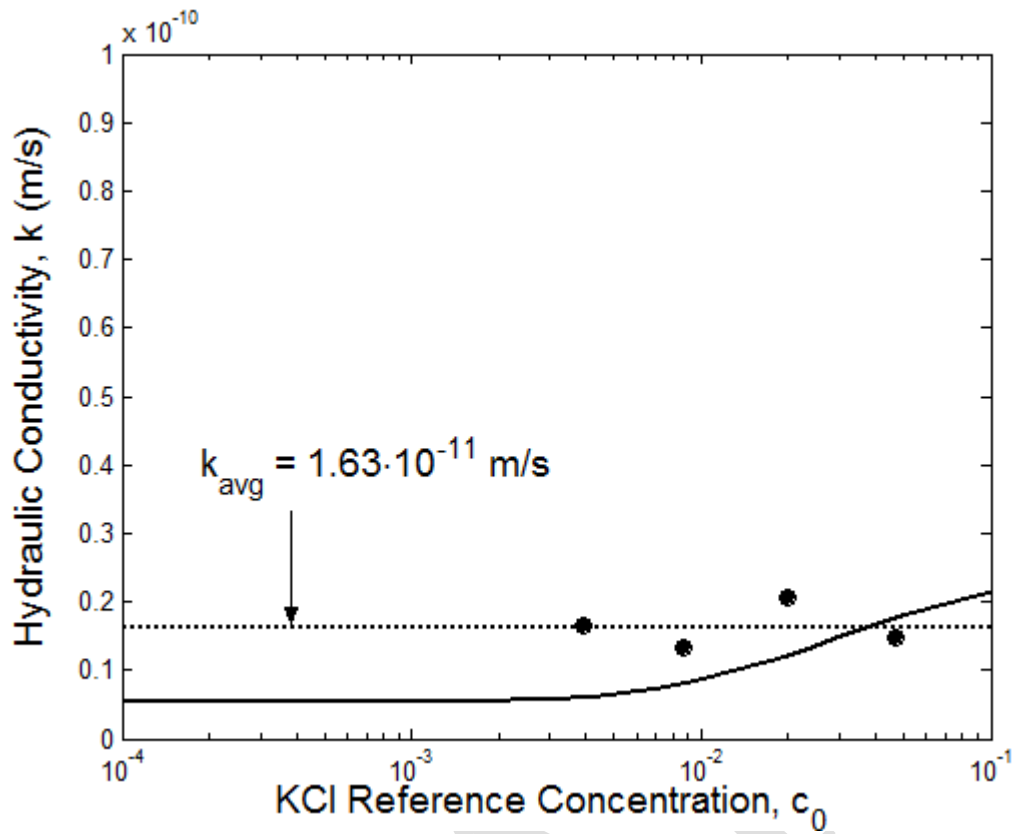
Figure 9. Hydraulic conductivity, k, determined on a GCL sample with porosity n = 0.79 by Malusis and Shackelford (2002a,b) as a function of the KCl reference concentration, c_0, and the theoretical interpretation (continuous line).
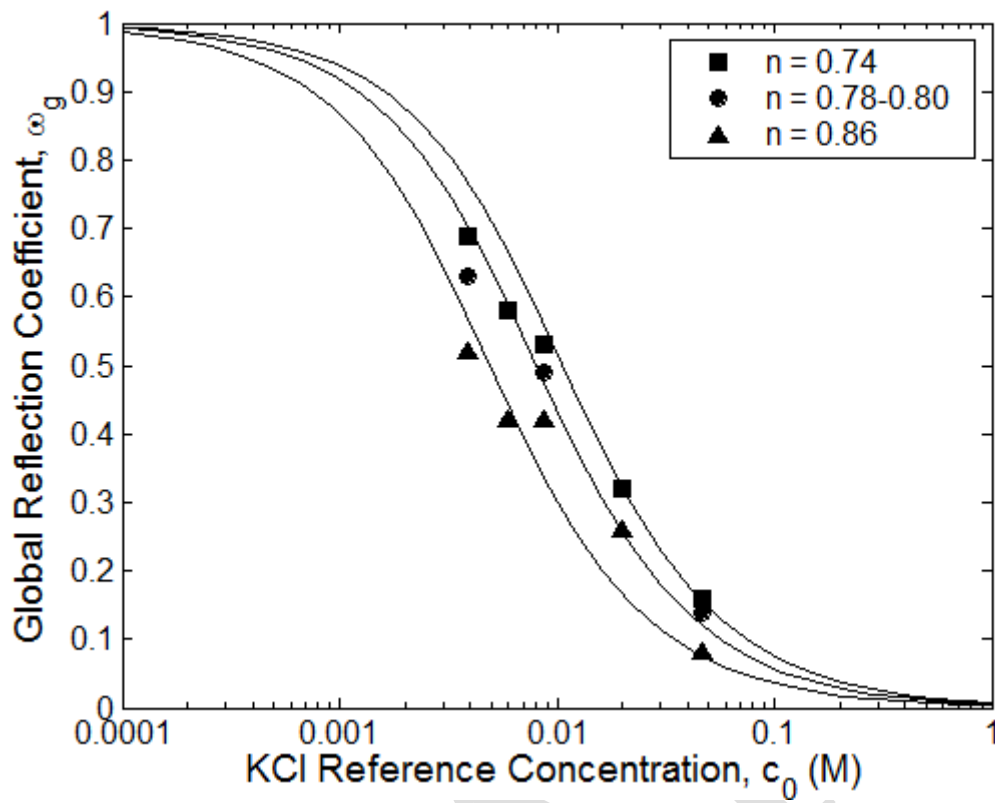
Figure 10. Global reflection coefficient ω_g measured by Malusis and Shackelford (2002a,b) on GCL samples as a function of the KCl reference concentration, c_0, and soil porosity, n, and the theoretical interpretation (continuous lines).
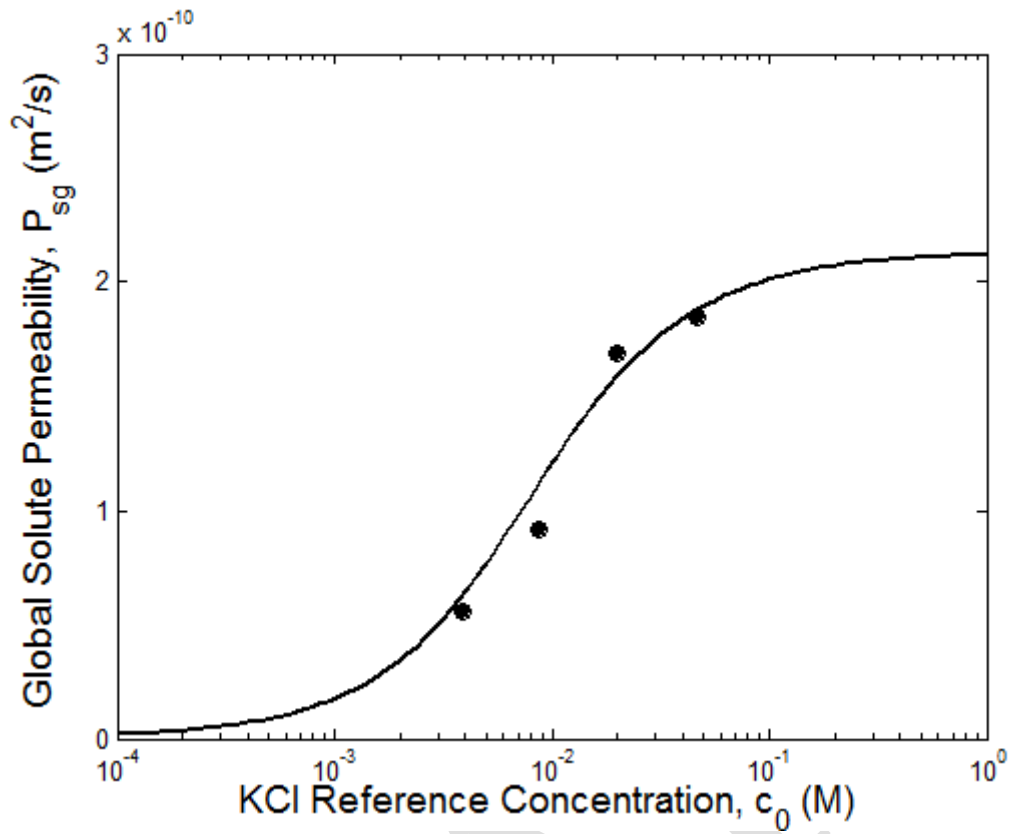
Figure 11. Global solute permeability, P_{sg}, determined on a GCL sample with porosity n =
0.79 by Malusis and Shackelford (2002a,b) as a function of the KCl reference concentration,
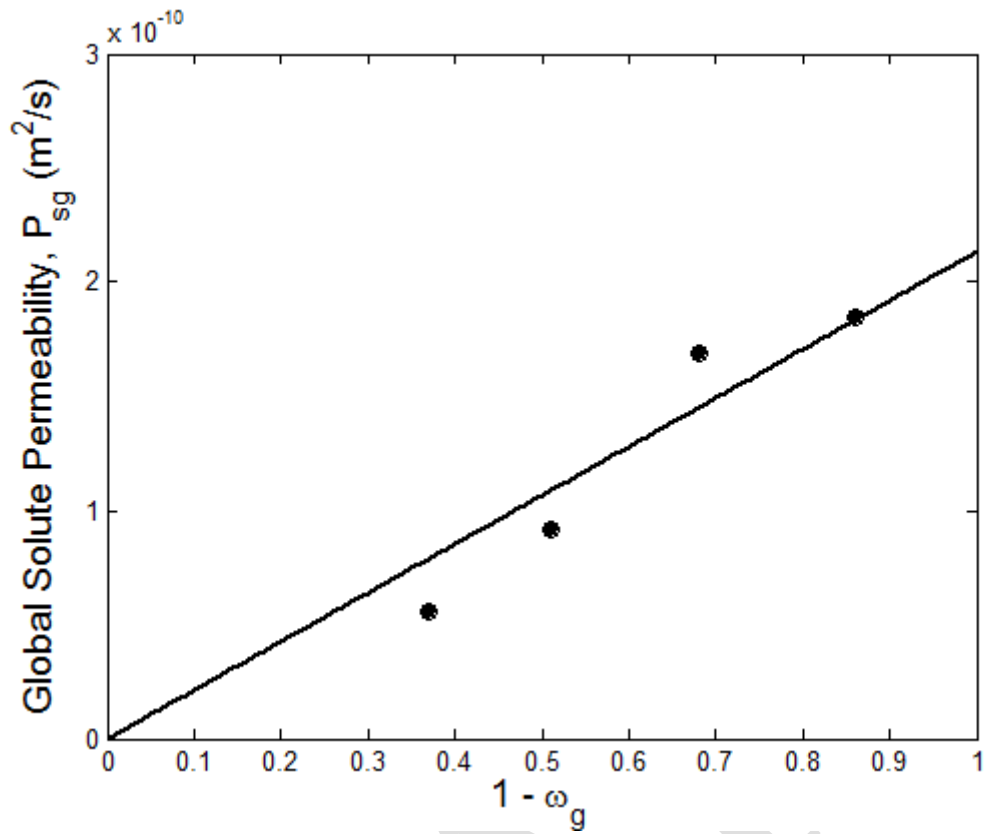c_0, and the theoretical interpretation (continuous line).

Figure 12. Global solute permeability, P_{sg}, as a function of the complement to 1 of the global reflection coefficient, ω_g, determined on a GCL sample with porosity $n = 0.79$ by Malusis and Shackelford (2002a,b) and the theoretical linear relationship (continuous line).
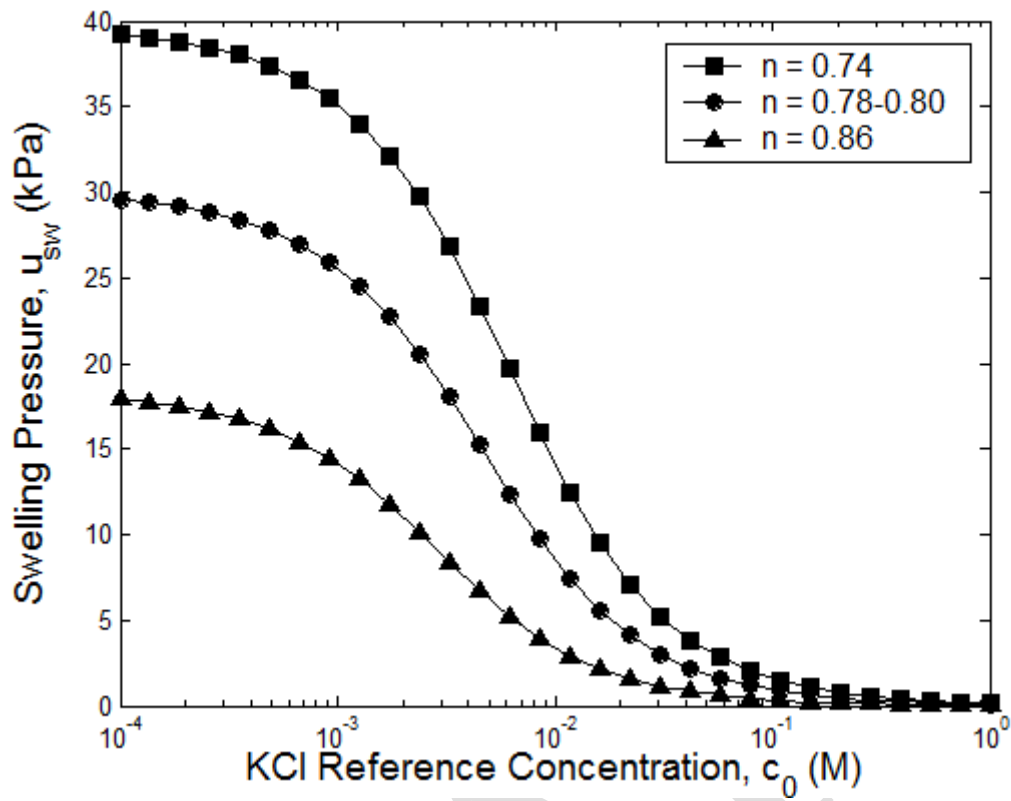
Figure 13. Theoretical swelling pressure, u_{sw}, as a function of the KCl reference concentration, c_0, and soil porosity, n, for the GCL investigated by Malusis and Shackelford (2002a,b). The theoretical curves have been derived from the equality of the reflection coefficient, ω, and the swelling pressure coefficient, ϖ, for a KCl solution ($D_{K,0} \cong D_{Cl,0}$).